JGR Biogeosciences

RESEARCH ARTICLE
10.1029/2020JG006191

Key Points:

- Spring physiological changes are examined using tower remote sensing data in a boreal mixed forest
- Evergreens reactivate in two phases. The second phase is synchronous with deciduous leaf-out
- Transition phases are controlled by air temperature, available soil water content, and soil thaw

Correspondence to:
Z. Pierrat and J. Stutz,
zpierrat@g.ucla.edu;
jochen@atmos.ucla.edu

Citation:
Pierrat, Z., Nehemy, M. F., Roy, A., Magney, T., Parazoo, N. C., Laroque, C., et al. (2021). Tower-based remote sensing reveals mechanisms behind a two-phased spring transition in a mixed-species boreal forest. *Journal of Geophysical Research: Biogeosciences*, *126*, e2020JG006191. https://doi.org/10.1029/2020JG006191

Received 4 DEC 2020
Accepted 31 MAR 2021

Author Contributions:

Conceptualization: Zoe Pierrat, Nicholas C. Parazoo, Colin Laroque, Katja Grossmann, Ulli Seibt, Jochen Stutz
Data curation: Magali F. Nehemy, Alexandre Roy, Alexandra Ramirez, Bruce Johnson, Warren Helgason, Alan Barr
Formal analysis: Zoe Pierrat, Magali F. Nehemy, Christoforos Pappas, Oliver Sonnentag, Alan Barr, Jochen Stutz
Funding acquisition: Zoe Pierrat, Troy Magney, Nicholas C. Parazoo, Colin Laroque, Ulli Seibt, Warren Helgason, Jochen Stutz
Investigation: Zoe Pierrat, Magali F. Nehemy
Methodology: Zoe Pierrat, Magali F. Nehemy, Alexandre Roy, Troy Magney, Colin Laroque, Christoforos Pappas, Katja Grossmann, David R. Bowling, Alexandra Ramirez, Alan Barr
Project Administration: Warren Helgason, Jochen Stutz
Resources: Jochen Stutz

Tower-Based Remote Sensing Reveals Mechanisms Behind a Two-phased Spring Transition in a Mixed-Species Boreal Forest

Zoe Pierrat[1], Magali F. Nehemy[2], Alexandre Roy[3], Troy Magney[4], Nicholas C. Parazoo[5], Colin Laroque[2], Christoforos Pappas[6,7], Oliver Sonnentag[6], Katja Grossmann[8], David R. Bowling[9], Ulli Seibt[1], Alexandra Ramirez[1], Bruce Johnson[2], Warren Helgason[2], Alan Barr[2], and Jochen Stutz[1]

[1]University of California Los Angeles, Los Angeles, CA, USA, [2]University of Saskatchewan, Saskatoon, SK, Canada, [3]Université du Québec à Trois-Rivières, Trois-Rivières, QC, Canada, [4]University of California Davis, Davis, CA, USA, [5]Jet Propulsion Laboratory, California Institute of Technology, Pasadena, CA, USA, [6]Centre d'étude de la forêt, Université du Québec à Montréal, Montréal, QC, Canada, [7]Département Science et Technologie, Téluq, Université du Québec, Montréal, QC, Canada, [8]University of Heidelberg, Heidelberg, Germany, [9]University of Utah, Salt Lake City, UT, USA

Abstract

The boreal forest is a major contributor to the global climate system, therefore, reducing uncertainties in how the forest will respond to a changing climate is critical. One source of uncertainty is the timing and drivers of the spring transition. Remote sensing can provide important information on this transition, but persistent foliage greenness, seasonal snow cover, and a high prevalence of mixed forest stands (both deciduous and evergreen species) complicate interpretation of these signals. We collected tower-based remotely sensed data (reflectance-based vegetation indices and Solar-Induced Chlorophyll Fluorescence [SIF]), stem radius measurements, gross primary productivity, and environmental conditions in a boreal mixed forest stand. Evaluation of this data set shows a two-phased spring transition. The first phase is the reactivation of photosynthesis and transpiration in evergreens, marked by an increase in relative SIF, and is triggered by thawed stems, warm air temperatures, and increased available soil moisture. The second phase is a reduction in bulk photoprotective pigments in evergreens, marked by an increase in the Chlorophyll-Carotenoid Index. Deciduous leaf-out occurs during this phase, marked by an increase in all remotely sensed metrics. The second phase is controlled by soil thaw. Our results demonstrate that remote sensing metrics can be used to detect specific physiological changes in boreal tree species during the spring transition. The two-phased transition explains inconsistencies in remote sensing estimates of the timing and drivers of spring recovery. Our results imply that satellite-based observations will improve by using a combination of vegetation indices and SIF, along with species distribution information.

Plain Language Summary

The boreal forest is one of the most sensitive regions on the planet to climate change, yet its sensitivity remains poorly understood. In particular, the timing and drivers of the spring transition, as the forest changes from a winter adapted state to a summer adapted state, carry significant uncertainties. Remote sensing metrics can be used to characterize the spring transition, but their interpretation is complicated by persistent greenness, frequent snow cover, and a high prevalence of forests containing both deciduous and evergreen species. We collected tower-based remotely sensed metrics, stem radius, and carbon uptake measurements and show that the spring transition occurs in two distinct phases. The first phase is a reactivation of photosynthesis in evergreens and is triggered by thawed stems, warm air temperature, and moist soil. The second phase is a change in evergreen photoprotective pigment levels and the leaf-out of deciduous species. It is triggered by soil thaw. Both phases were detected with different remote sensing metrics that depended on species type. Our results illustrate how satellite measurements could be improved to capture the spring transition over diverse landscapes and what environmental factors control the spring transition.

Software: Zoe Pierrat, Katja Grossmann, Jochen Stutz
Supervision: Troy Magney, Nicholas C. Parazoo, Colin Laroque, Oliver Sonnentag, David R. Bowling, Jochen Stutz
Writing – original draft: Zoe Pierrat, Magali F. Nehemy, Alan Barr
Writing – review & editing: Zoe Pierrat, Magali F. Nehemy, Alexandre Roy, Troy Magney, Nicholas C. Parazoo, Colin Laroque, Christoforos Pappas, Oliver Sonnentag, Katja Grossmann, David R. Bowling, Ulli Seibt, Alan Barr, Jochen Stutz

1. Introduction

The boreal forest is a major contributor to the global carbon and water cycles and is one of the region most sensitive to environmental change (Bonan, 2008; Thurner et al., 2014). Climate change has led to an earlier spring onset and longer growing season, but the potential impacts of this change on the annual carbon balance and seasonal vegetation phenology remain uncertain (Fisher et al., 2018; Fu et al., 2017; Goetz et al., 2005; Richardson et al., 2010; Schaefer et al., 2014). Contributing to this uncertainty, global climate models currently fail to accurately predict the onset of spring photosynthesis (Commane et al., 2017; Parazoo et al., 2018; Peng et al., 2014; Richardson et al., 2012). This is partly due to difficulties in accurately measuring the onset of spring photosynthesis through remotely sensed products, and partly due to uncertainties in understanding the environmental controls on the timing and rate of spring photosynthetic recovery (Jeong et al., 2011, 2017). Overcoming these challenges is, therefore, critical for understanding the fate of the boreal region in the context of climate change.

Studying the boreal forest spring recovery is challenging, in large part, because it has widespread mixed forest stands with both deciduous and evergreen species. Trees within these stands experience the same environmental conditions but exhibit vastly differing life strategies in both their short-term (daily) functioning (Pappas et al., 2018) and their long-term (monthly) seasonal dynamics (Reich, 2014). During fall, deciduous species drop their leaves and go into a long-term winter dormancy before regrowing them in the spring. This strategy allows deciduous plants to avoid both damage due to freezing and photodamage caused by the absorption of winter sunlight which they are unable to use to drive photosynthesis. Evergreen trees, on the other hand, retain their needles, and must undergo biochemical changes to downregulate photosynthesis in the winter months while still absorbing appreciable sunlight (Ensminger et al., 2004). To do this, evergreens transition from rapidly reversible non-photochemical quenching (NPQ), typical of summer, to sustained NPQ for winter by changing their photoprotective pigments associated with the xanthophyll cycle (Adams et al., 2004; Verhoeven, 2014). During winter, to support sustained NPQ, needles accumulate and retain zeaxanthin, and there is an overall increase in the xanthophyll pigment pool size (Gilmore & Ball, 2000). Therefore, in spring, evergreens decrease their bulk carotenoid pigments (including xanthophyll pigments), but maintain high levels of zeaxanthin and antheraxanthin so they can rapidly shift their photoprotective state during the day for protection during high light conditions. Throughout the year, changes in chlorophyll can be much smaller than changes in carotenoid pigments (Bowling et al., 2018; Gilmore & Ball, 2000) and as a result, there is an increase in the ratio of chlorophyll to carotenoid pigments (Chl:Car) in spring and a decrease in winter (Adams et al., 2002; Oh et al., 2013; Öquist & Huner, 2003; Ottander et al., 1995). The difference in the spring recovery process between evergreen and deciduous species, and the multiple biochemical processes evergreen species undergo, has led to several remotely sensed products, from the leaf to the satellite scale, to investigate the spring transition, each with their own advantages and disadvantages.

Greenness based indices such as the Normalized Difference Vegetation Index (NDVI) and the Near-Infrared Reflectance from Vegetation (NIRv), among others (EVI, GEMI, SAVI, etc.), have been used to successfully track vegetation cover and productivity across biomes (Badgley et al., 2019; Tucker, 1979). NDVI provides an estimate of canopy chlorophyll content in a pixel and therefore tracks the spring onset well in deciduous forests and grasslands (Wang et al., 2019; Yang et al., 2017). However, NDVI is sensitive to non-vegetated surfaces such as clouds, snow, and water, and saturates at high leaf area index (LAI), all of which present challenges for decoupling vegetation productivity from other artifacts that are particularly present in the boreal forest (Gamon et al., 2013). NIRv goes a step beyond NDVI in that it isolates the vegetated signal by amplifying the near-infrared reflectance and is, therefore, less sensitive to snow cover and other confounding signals (Badgley et al., 2017, 2019). However, greenness based indices do not provide plant functional information related to photosynthetic activity or light use efficiency (LUE) (Gitelson & Gamon, 2015). Therefore, they may fail to capture the photosynthetic activity of evergreen species that remain green year round despite a complete downregulation of photosynthesis (Magney, Bowling, et al., 2019; Badgley et al., 2019; D. A. Sims et al., 2006; Garbulsky et al., 2010).

Two other vegetation indices, the Photochemical Reflectance Index (PRI) and the Chlorophyll Carotenoid Index (CCI), are also promising metrics for detecting seasonal changes in evergreen photosynthesis because they are connected to photosynthetic phenology of evergreen conifers and have been shown to be viable indices for tracking seasonal photosynthetic activity at leaf and canopy scales for evergreen species (Gamon

et al., 1992, 2016; Springer et al., 2017; Wong & Gamon, 2015a). PRI acts as an indicator of short-term xanthophyll cycle activity while CCI is sensitive to the seasonal behavior of bulk carotenoid pigment pools - including the seasonal retention of xanthophyll pigments (Gamon et al., 1992, 2016). However, several studies have shown that PRI can vary substantially over longer time scales and the PRI/LUE relationship can change dramatically under changing environmental conditions such as altered nutrient status, (Gamon et al., 1997), water status (Filella et al., 2004; D. Sims et al., 2006), and temperature (Porcar-Castell et al., 2012). Furthermore, variability in PRI across different species outweighs biochemical responses of PRI in one species (Atherton et al., 2017). This poses a significant challenge for spatially averaged measurements over mixed forest stands where changes in PRI could merely reflect changes in species breakdown. These potentially confounding and decoupled effects pose significant challenges for using PRI and/or CCI to determine the spring transition.

Finally, Solar-Induced Chlorophyll Fluorescence (SIF) is the small emission of red and far-red light from excited chlorophyll-a molecules. It is frequently used as a proxy for GPP and has been used to represent the timing of spring GPP onset in Alaskan ecosystems from satellite measurements (Commane et al., 2017; Jeong et al., 2017; Luus et al., 2017; Parazoo et al., 2018; Walther et al., 2016). These satellite measurements, however, are spatially averaged over multiple vegetation types at a much coarser spatial resolution than traditional vegetation indices (e.g., 10–500 m for Sentinel and MODIS reflectance; 2–500 km for OCO2, TROMOMI, GOME-2 SIF). Satellite SIF is, therefore, more susceptible to mixing species specific information within the spring transition. In addition, spatial averaging is often inconsistent between satellites, thus worsening the problem. In fact, satellite-based morning overpasses show a delay in SIF onset relative to daily mean GPP from towers (Parazoo et al., 2018). In contrast, tower-based measurements of SIF have shown slight increases in SIF preceding changes in GPP, suggesting respiratory recycling of CO_2 before water transport and stomatal opening (Magney, Bowling, et al., 2019). These contrasting results highlight the need for a more in-depth investigation of the linkages between SIF and carbon uptake during the spring transition.

To verify these remotely sensed products, photosynthesis, carbon uptake, and other plant functions can be locally inferred by eddy-covariance (EC) measurements (Baldocchi et al., 1988) as well as tree-specific stem radius measurements (Drew & Downes, 2009). EC measurements of net ecosystem exchange (NEE), and derived measurements of GPP, can be used to study reactivation of photosynthetic function. However, EC derived GPP is subject to large uncertainties, particularly during the spring transition in arctic ecosystems and mixed forest stands where initial fluxes can be especially small relative to the growing season maximum (Baldocchi, 2003; Parazoo et al., 2018). Within the EC footprint, the spring recovery of understory, deciduous, and evergreen species is captured in a spatially averaged product that cannot distinguish between species-specific recovery (Baldocchi, 2003). Therefore, EC derived GPP measurements are less effective at probing the species-dependent recovery of the widespread mixed forest stands found in the boreal region. Assessment of stem radius change with dendrometers, on the other hand, provides hourly resolution, tree-specific measurements of growth and tree water relations (Steppe et al., 2006; Zweifel, 2016; Zweifel & Häsler, 2001). Stem radius measurements have been widely recognized as a useful indicator of drought stress but have more recently been used to study fundamental mechanisms underlying whole-plant functioning and growth (De Swaef et al., 2015). Stem radius change measurements can provide information on water uptake by trees during winter (Sevanto et al., 2006) and reveal a shift to springtime stem re-hydration (Turcotte et al., 2009). Therefore, stem radius measurements can allow us to better understand the species-specific spring recovery in mixed forest stands. Finally, the timing of the onset of growth from stem radius measurements provides additional valuable information on long-term sequestration of carbon and how this may change under future climate scenarios (Zweifel et al., 2010).

The variety of remotely sensed products and potential limitations of spatially integrated GPP measurements have led to large uncertainties in the timing of the spring recovery in needleleaf forests, and a broad range of proposed environmental controls for what drives this recovery. Proposed drivers include warmer air temperatures, increases in plant available soil water content, photoperiod, and thawing stems, needles, and soils (Ensminger et al., 2004; Öquist & Huner, 2003; Parazoo et al., 2018; Tanja et al., 2003; Wu et al., 2013). The exact controls of the spring recovery, however, remain uncertain (Ensminger et al., 2004). By understanding how evergreen and deciduous species respond to the spring recovery separately, we can better understand the information contained in spatially integrated remote sensing measures and more accurately determine

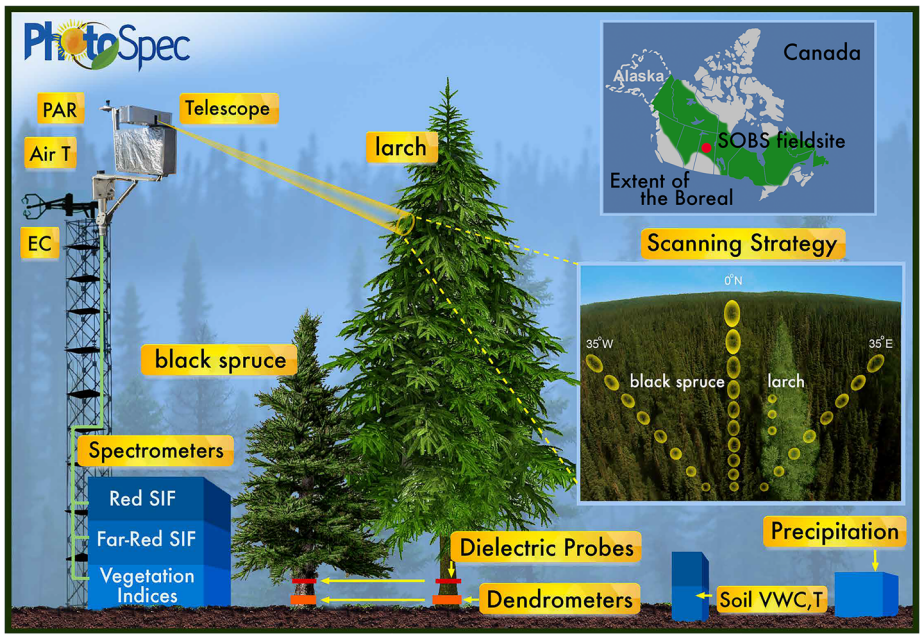

Figure 1. Field site location with PhotoSpec and support measurements at the Southern Old Black Spruce (SOBS) site in Saskatchewan, Canada. PhotoSpec set up is shown with an inset of the scanning strategy and measurement points on both black spruce and larch.

the specific environmental controls relevant for the recovery of each species. Therefore, our ability to accurately determine the timing and drivers of the onset of the spring transition depends on our ability to utilize remote sensing metrics sensitive to physiological changes occurring in the boreal forest during this time.

The goal of this study is to explore how we can best utilize existing sets of remote sensing metrics, to better characterize the timing and drivers of the spring transition in a boreal mixed forest. This includes utilizing a multivariate approach combining tower-based remote sensing with tree-level ecophysiological data to characterize: the onset of photosynthesis, pigment transitions, deciduous leaf-out, stem rehydration, the onset of transpiration, and the start of radial wood growth for individual species. Specifically, we seek to answer:

1. How can tower-based remote sensing products be used to determine the spring transition and what physiological mechanisms are they sensitive to?
2. What environmental conditions are driving changes in photochemical and biochemical regulation of the spring transition?

We explore the efficacy of remotely sensed metrics (NDVI, NIRv, PRI, CCI, and SIF) for determining the spring transition for both deciduous and evergreen species in the boreal forest. We compare co-located and concurrently recorded tower-based remote sensing metrics and ground measurements of stem radius change and tower-based measurements of GPP, all collected at a half-hourly resolution, to determine relevant physiological changes during the spring transition, and which of these changes can be measured with remote sensing. Using this information, we examine different environmental conditions that drive various stages of the spring transition. We used a random forest model to quantify the importance of different environmental conditions and qualitatively connected these conditions to periods of increased productivity to provide an explanation for what controls the spring transition.

2. Materials and Methods

2.1. Site Description: Southern Old Black Spruce

The study site (Southern Old Black Spruce, SOBS, Fluxnet ID CA-Obs) is located near the southern limit of the boreal forest ecotone in Saskatchewan, Canada (53.98°N, 105.12°W) (Figure 1). It is a mixed forest stand with stem density predominantly (90%) black spruce (*Picea mariana*), and scattered (10%) larch

(*Larix laricina*) (Pappas, Maillet, et al., 2020). Average canopy height at the site is ~16 m for larch and ~11 m for black spruce with a canopy leaf area index of ~3.8 m^2 m^{-2} (Chen et al., 2006). Wild rose (*Rosa woodsii*) and Labrador tea (*Ledum groenlandieum*) are the main understory vegetation, with ground cover consisting mainly of mixed feather mosses (*Hylocomium splendens*, *Pleurozium schreberi*, and *Ptilium crist-acastrensis*), with some peat moss (*Sphagnum* spp.) and lichen (*Cladina* spp.) (Gaumont-Guay et al., 2014). The soil is moderately-to-poorly drained with a 20–30 cm thick peat layer overlying waterlogged sand. The site is equipped with a twin scaffold tower at 25 m above ground level (agl), approximately twice the height of the forest canopy.

2.2. Remote Sensing: PhotoSpec

We collected co-located remotely sensed products (NDVI, NIRv, PRI, CCI, red SIF, and far-red SIF) using PhotoSpec (see Grossmann et al., 2018 for detailed instrument description) in the spring of 2019 and 2020. PhotoSpec was installed at the top of the scaffolding tower (25 m agl) facing due north. It has a narrow field of view (0.7°) and a 2-D scanning capability which permits independent measurements of both black spruce and larch, giving it a unique advantage over spatially averaged satellite measurements. Our scanning strategy had three "elevation scans" (scanning vertically) at 35°W (10 measurements), 0°N (24 measurements), and 35°E (10 measurements) that observed predominantly black spruce and three individual targets on a larch (Figure 1). Individual measurements take approximately 20 s and the complete scan cycle repeats on a 30 min loop.

Vegetation indices were calculated as the following, with $\rho_{nm:nm}$ = the average reflectance across a wavelength range in nm:

$$NDVI = (\rho_{830:860} - \rho_{620:670})/(\rho_{830:860} + \rho_{620:670})$$ (Tucker, 1979)

$$NIRv = (\rho_{830:860} - \rho_{620:670})/(\rho_{830:860} + \rho_{620:670})^{*}\rho_{830:860}$$ (Badgley et al., 2017)

$$PRI = (\rho_{569:571} - \rho_{520:532})/(\rho_{569:571} + \rho_{520:532})$$ (Gamon et al., 1992)

$$CCI = (\rho_{520:532} - \rho_{620:670})/(\rho_{520:532} + \rho_{620:670})$$ (Gamon et al., 2016)

SIF was retrieved in the red (680–686 nm) and far-red (745–758 nm) wavelength ranges using a Fraunhofer-line based retrieval (Grossmann et al., 2018). Retrieval errors are calculated as outlined in Grossmann et al. (2018) and propagated through any calculation in this study. Our retrieval approach is comparable to those in Magney, Bowling, et al. (2019); Magney, Frankenberg, et al. (2019); He et al. (2020). To decouple the physical (light, structure, viewing, and solar geometries) from the physiological SIF signal, and account for variations in incident light and sun/shade fraction within the field of view, we calculated $SIF_{relative}$ (a proxy for SIF_{yield}) in both the red and far-red wavelength ranges as: $SIF_{relative} = SIF/I$, Where I is the near-infrared (NIR) radiance in the SIF retrieval window (680–686 nm for red and 745–758 nm for far-red), for example, (Parazoo et al., 2020; Magney, Frankenberg, et al., 2019).

We collected 1 s Photosynthetically Active Radiation (PAR) data and used these data to remove PhotoSpec measurements where PAR conditions changed significantly ($PAR_{std} > 0.2 \times PAR_{avg}$) over the PhotoSpec integration time. We then filtered all data points for NDVI > 0.5 in order to remove points that were mostly obscured by snow or non-green vegetation (soil, branches, and stems), although this process left some measurements with mixed pixels. A lower NDVI threshold (NDVI > 0.2) did not change results of our study and merely increased the scatter and snow responses of vegetation indices. We excluded low-quality retrievals where the SIF retrieval error was >0.1 W m^{-2} sr^{-1} μm^{-1} and where SIF < −0.1 W m^{-2} sr^{-1} μm^{-1} or SIF > 10 W m^{-2} sr^{-1} μm^{-1}. Finally, we only considered data where the Solar Zenith Angle (SZA) < 80° to remove data where low light conditions increase retrieval uncertainty.

We calculated species specific averages over each 30 min period which were again averaged to report daily averages of $SIF_{relative}$ and reflectance measurements for both black spruce and larch in 2019 and 2020 (Figures 2 and 3).

Finally, days with significant snow cover, were identified visually using phenocam images at the site (https://phenocam.sr.unh.edu/webcam/sites/canadaOBS/) and highlighted in Figures 2 and 3. Our filtering strategy allowed us to effectively isolate remote sensing pixels predominantly filled with plants and identify periods with potential snow contamination.

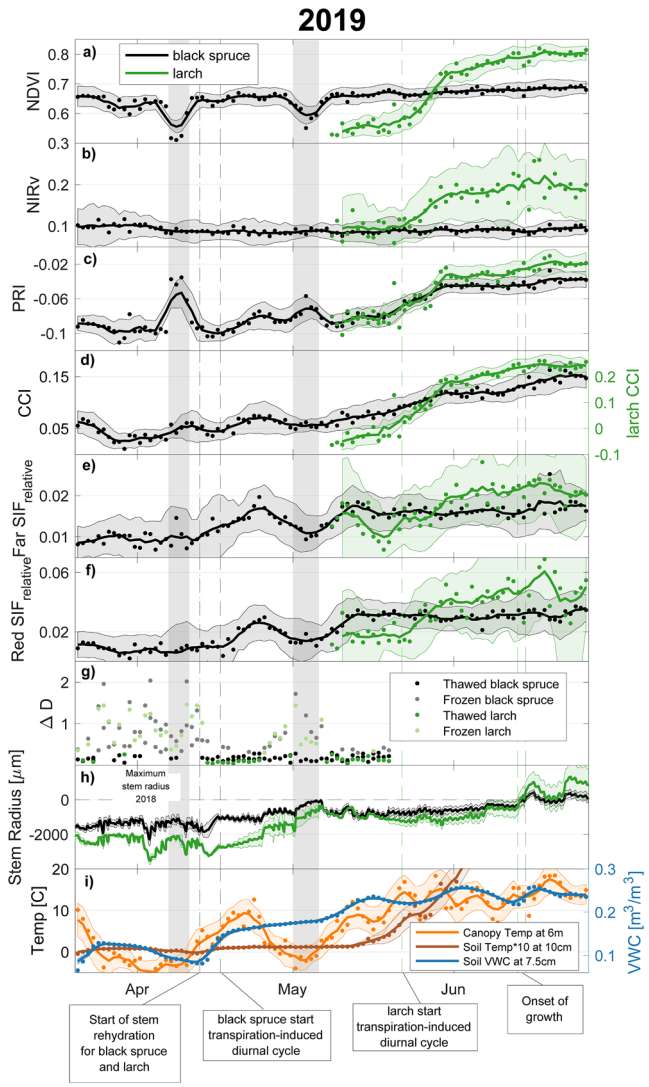

Figure 2. Data collected for the 2019 spring transition for both black spruce and larch. Periods of snow cover are shaded in gray. (a)–(f) show daily averaged PhotoSpec remotely sensed products with a 5 days moving mean. Shaded error bars are the 5 days moving mean of twice the standard deviation of the diurnal variability. (g) shows the daily range in the dielectric constant. (h) shows stem radius measurements. The zero line is the maximum stem radius from 2018. Shaded regions are twice the standard deviation among species specific dendrometers. (i) shows daily average environmental conditions.

2.3. Tree Water Status

2.3.1. Freeze/Thaw State: Dielectric Probes

The freeze-thaw state of the tree trunks was determined with dielectric probes inserted into three tree trunks (two black spruce, one larch). Three ruggedized soil moisture sensors (model GS-3; Decagon Devices) were installed directly into 5.6 cm pre-drilled holes (length of probes) within tree trunks, in order to provide a measure tree relative dielectric constant and tree skin surface temperature. The probes are sensitive to liquid water, as liquid water has a near constant dielectric constant compared to frozen water. The dielectric constant (D) follows ambient temperature in winter but is near constant when trunks are thawed in the spring (Matheny et al., 2015; Roy et al., 2020). We defined a daily range in the dielectric constant, $\Delta D = D_{max} - D_{min}$, and classified trunks as frozen for $\Delta D > 0.3$ and thawed for $\Delta D < 0.3$ in 2019 and frozen for $\Delta D > 0.5$ and thawed for $\Delta D < 0.5$ in 2020 after reinstalling following probe failures in 2019. Re-calibration of the ΔD threshold in 2020 yielded no significant difference in the results.

2.3.2. Stem Radius: Dendrometers

We monitored stem radius change of 13 black spruce and 13 larch trees to determine water storage dynamics and the onset of transpiration. We used automatic dendrometers (DC3; Ecomatik) to obtain half-hourly measurements of stem radius change at breast height. The data were recorded using HOBOUX120-006M data loggers, where each logger was connected to four dendrometers. The average stem diameter at breast height of monitored trees was 13 cm for black spruce and 18 cm for larch. We converted dendrometer measurements to μm and corrected for thermal sensitivity according to manufacturer's specifications. The recorded data were further processed to identify errors and sensor malfunctioning as a result of wildlife chewing wires, logger battery failure, and moisture interference. Identified periods of sensor malfunction and abnormal jumps were removed creating gaps in the specific sensor data record, which remained unfilled.

We investigated stem radius diurnal cycles and hydraulic signals to determine the timing of stem re-hydration and the onset of transpiration in the spring following the empirical approach proposed by King et al. (2013). We obtained diurnal cycle information by subtracting the daily mean from each measurement and removing growth trend. This provides only reversible stem radius change, attributable to tree water relations. In winter, when trees are dehydrated, the mean stem diurnal cycle shows a negative sinusoidal phase with patterns of minimum stem radius observed in the morning and maximum stem radius observed in the afternoon (daytime SR_{max} & nighttime SR_{min}). This cycle reflects changes in temperature as it induces nighttime frost-shrinkage and daytime bark swelling (Ameglio et al., 2001; Kozlowski & Winget, 1964; Loris et al., 1999; Tardif et al., 2001; Zweifel & Häsler, 2000) and is an important mechanism for winter acclimation (Pearce, 2001; Wisniewski et al., 2014). During the growing season, the mean stem diurnal cycle reverses and follows a positive sinusoidal phase which reflects the balance between water loss from transpiration at the canopy level and water uptake from the soil through the roots at night (Kozlowski & Winget, 1964; Zweifel & Häsler, 2001). Therefore, trees experience stem expansion at night when they refill internal storage and stem shrinkage during the day as water stores are depleted by transpiration that increases the tree water deficit (daytime SR_{min} & nighttime SR_{max}) (Steppe et al., 2006; Zweifel et al., 2016). Thus, tree radius varies daily because of transpiration-induced changes in water storage and potential in the stem (Perämäki et al., 2001). We used the shift in the diurnal cycle of

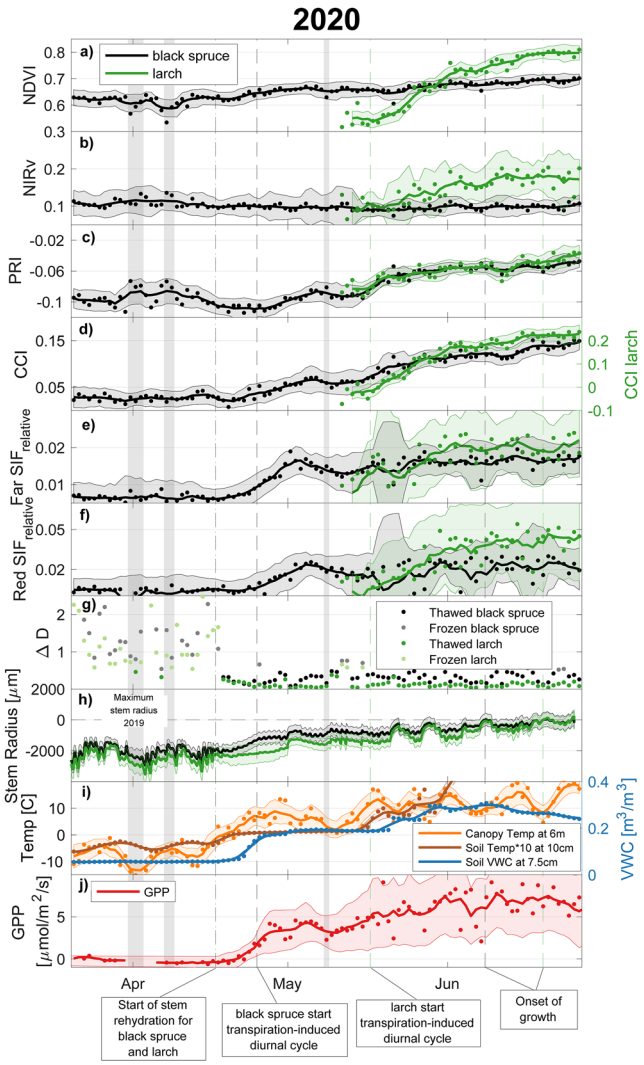

Figure 3. Data collected for the 2020 spring transition for both black spruce and larch. Periods where snow cover obscured remotely sensed products are shaded in gray. (a)–(i) are the same as Figure 2, but for 2020. (j) shows daily average GPP.

tree trunk radii to indicate the onset of transpiration in the spring (King et al., 2013; Pappas, Peters, & Fonti, 2020; Sevanto et al., 2006).

We infer radial growth of the trees following the zero-growth (ZG) approach (Zweifel et al., 2016). The ZG approach defines radial growth as the difference between the current measured stem radius (SR_t) and the maximum measured stem radius in the past (SR_0), so that $SR = SR_t - SR_0$. We determined the onset of radial growth when SR exceeded the maximum radii from the previous growing season ($SR > 0$). The extracted growth signal is the total radial increment in tree diameter in μm per day. This approach assumes that radial growth only occurs when trees are fully hydrated without water deficit. This approach results in comparable patterns to other methods to determine tree radial growth (Eller et al., 2018).

2.4. Gross Primary Production

Eddy-covariance (EC) measurements of net ecosystem exchange (NEE) (μmol C m^{-2} s^{-1}) and friction velocity u* (m s^{-1}) were made from atop the site's 25 m scaffold tower. The EC system consisted of a 3-D sonic anemometer (CSAT3, Campbell Scientific) in combination with a closed-path infrared gas (CO_2/H_2O) analyzer (LI-7200 analyzer, Li-Cor) operated in absolute mode. The 30-min eddy fluxes were computed using the Eddy-Pro software (version 7.0.6, Li-Cor). NEE was calculated as the sum of the measured CO_2 eddy flux at the instrument height and the change in CO_2 storage in the air layer between the instruments and the surface (Barr et al., 2006). Nighttime NEE values were rejected under calm conditions using a u* threshold of 0.30 m s^{-1}. Net Ecosystem Production (NEP) was estimated as -NEE assuming no losses via dissolved organic carbon. Finally, gaps in NEP were filled and NEP was partitioned into gross primary production GPP (μmol C m^{-2} s^{-1}) and total ecosystem respiration R_e (μmol C m^{-2} s^{-1}) using the standard Fluxnet-Canada method (Barr et al., 2004). After processing, we report daily average GPP for only 2020 (Figure 3j), as 2019 GPP data were not recorded.

2.5. Environmental Variables

Air temperature and relative humidity were recorded in the canopy at 6 m height with a Vaisala HMP45C probe. Soil temperature measurements were taken with Type-T (copper-constant) thermocouples at two locations at a 10 cm depth below the living-moss layer and averaged together. Soil volumetric water content (VWC) was recorded at two locations at a 7.5 cm depth with Cambell Scientific CS615 Water Content Reflectometers and averaged together. Vapor pressure deficit (VPD) was calculated from air temperature and relative humidity. All environmental variables were recorded at a 30 min time resolution and averaged together for daily resolution.

3. Results and Discussion

3.1. Remote Sensing and Stem Radius Results

Daily time series of vegetation indices, $SIF_{relative}$, ΔD, stem radius, environmental conditions, and GPP in 2019 and 2020 are presented in Figures 2 and 3, respectively. Snow days (as identified with phenocam images) are highlighted with shaded vertical gray bars. Important transitions in stem radius and water use are identified with vertical dashed lines and expanded upon in Figures 4, 5 and 6. Shaded error bars indicate the 5 days moving mean of twice the standard deviation of diurnal variability. In general, larch exhibit a larger

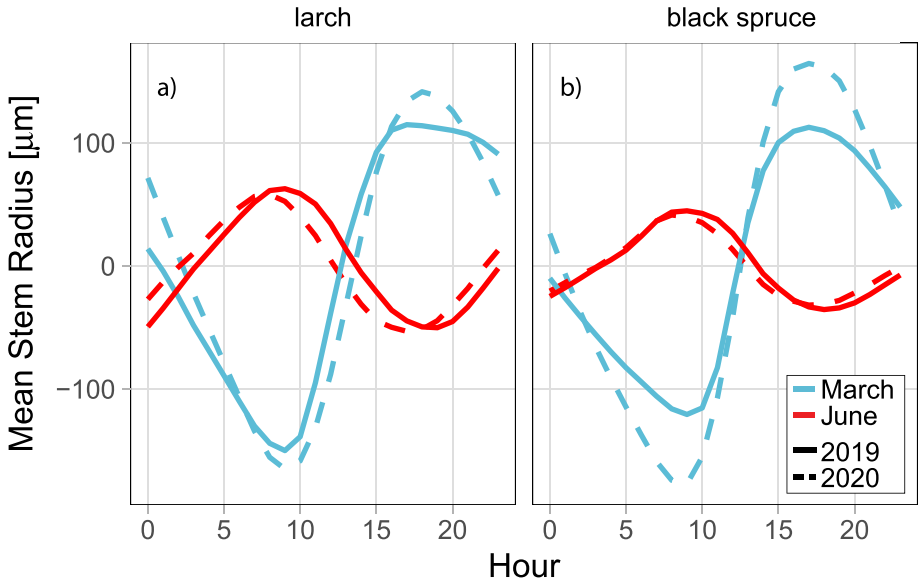

Figure 4. Mean monthly diurnal cycle of larch (a) and black spruce (b) in 2019 and 2020. Data show temperature driven diurnal cycle during March (winter) and a reversed pattern in June (summer) showing transpiration-induced cycle.

standard deviation than spruce due to a more limited number of data points. Our results highlight the large seasonal differences between black spruce and larch and the variations between remotely sensed products.

During the winter to spring transition, NDVI and NIRv are relatively invariant for black spruce but show rapid increases during larch leaf-out (Figures 2a, 2b, 3a, and 3b). Black spruce NDVI decreases as a response to snow days, despite filtering for NDVI > 0.5. These snow dates occur on April 7–10 and May 1–5 in 2019 (Figure 2a) and March 31–April 2, April 7 & 8, and May 8 in 2020 (Figure 3a). NIRv in black spruce does not show snow variability (Figures 2b and 3b). Larch leaf-out on May 22 in 2019, and May 17 in 2020 was captured with NDVI and NIRv and is supported by visual inspection of the Phenocam data (Figures 2a, 2b, 3a, and 3b).

PRI, CCI, red and far-red $SIF_{relative}$ show ecophysiologically relevant changes for both black spruce and larch (Figures 2c–2f and 3c–3f). Black spruce PRI increases as a response to snow cover in 2019 and 2020 (Figures 2c and 3c). In 2020, these responses are more subtle in the 5-day moving mean because periods of snow cover are much shorter than in 2019. Black spruce PRI increases slightly beginning April 17, 2019 and April 25, 2020, followed by large increases beginning May 22, 2019 and May 17, 2020. The PRI signal then levels off by June 1, 2019 and May 25, 2020. For larch, changes in PRI closely follow the timing of the leaf-out in both 2019 and 2020. CCI shows remarkably similar patterns to PRI, however, it is unaffected by snow cover in both 2019 and 2020. Black spruce CCI shows small increases beginning April 17, 2019 and April 25, 2020, that coincide with the small changes in PRI. CCI then decreases slightly in 2019 and levels off in 2020 for a short period of time, before increasing again around May 22, 2019 and May 17, 2020. This second increase in CCI is largely consistent with the larch leaf-out and the second increase in PRI. Larch CCI again follows the timing of the leaf-out (Figures 2d and 3d). Black spruce red and far-red $SIF_{relative}$ increase prior to larch leaf-out in both 2019 and 2020 (Figures 2e, 2f, 3e, and 3f). In 2019, $SIF_{relative}$ begins to increase starting April 17 and continues to increase through April 25. After April 25, $SIF_{relative}$ decreases through May 5 before increasing again and leveling off by May 13 (Figure 2e and 2f). In 2020, $SIF_{relative}$ begins to increase on April 25 and continues to increase through May 2. $SIF_{relative}$ then decreases slightly May 2 through May 11, before increasing again slightly and leveling off by May 15 (Figure 3e and 3f).

The daily range in the dielectric constant, ΔD, shows periods of frozen and thawed stems. In 2019, stem thaw began April 13, followed by a brief freeze starting April 25, and a thaw again on May 6 (Figure 2g). One of the black spruce trees remained thawed through the April 25–May 6 re-freeze, which suggests an

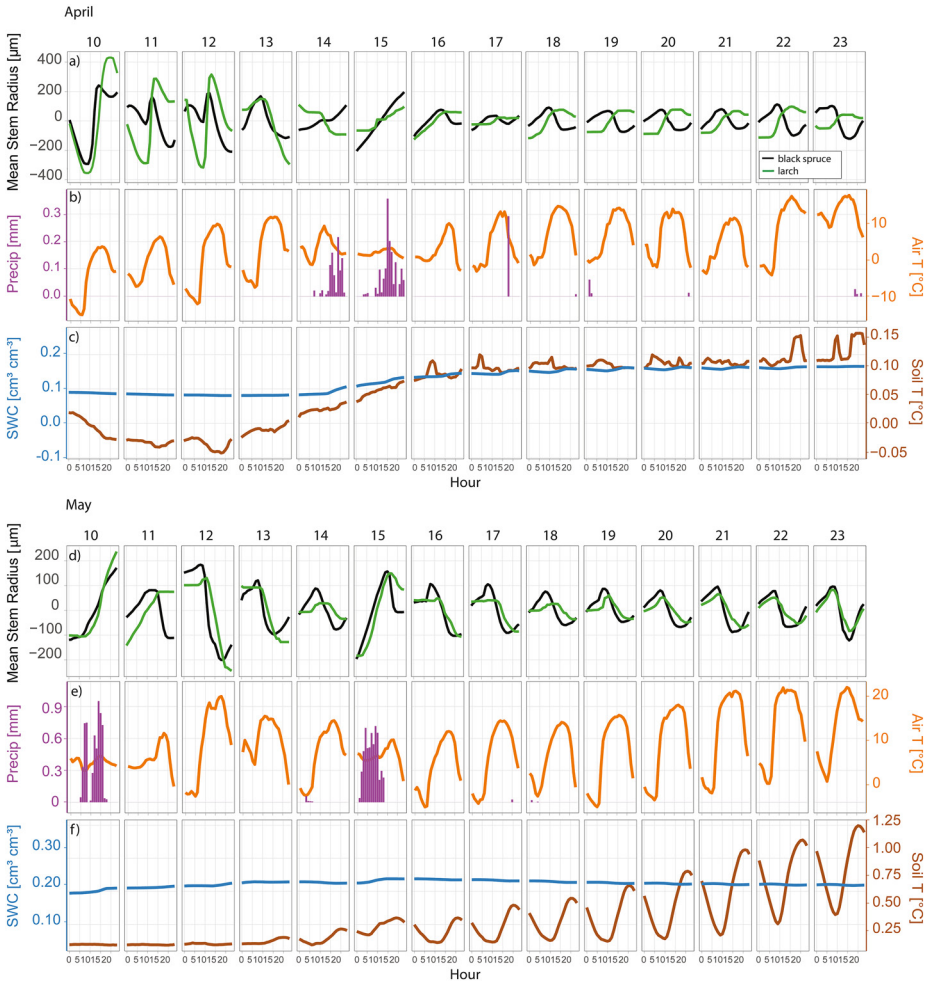

Figure 5. Half-hourly mean environmental variables and stem diurnal cycle during the onset of transpiration in April ((a)–(c)) and May ((d)–(f)) 2019. Panel (a) and (d) show mean stem radius (Mean SR) for black spruce and larch. Panel (b) and (e) show precipitation (Precip) and air temperature (Air T) during same time interval. Lower panels show soil volumetric water content (SWC) and soil temperature (Soil T). The number on the top of each panel indicates the day of the month. SWC, soil volumetric water content.

uneven freeze-thaw distribution among trees, although with only three points sampled this may merely be a reflection of tree diameter at the measurement point. In 2020, stem thaw occurred April 18 and stems remained thawed with a few exceptions on May 11, 12, and 15 (Figure 3). The freeze-thaw state of the stems in both 2019 and 2020 closely follows increases and decreases in air temperature (Figures 2i and 3i) as well as increases and decreases in $SIF_{relative}$ in black spruce.

Investigation of stem radius change shows typical patterns for winter and summer in both black spruce and larch in 2019 and 2020. Monthly average diurnal cycle (Figure 4) shows a temperature-driven diurnal cycle in March, and a transpiration-induced cycle in June. King et al. (2013) observed similar patterns in diurnal cycle of Norway spruce (*Picea abies*) and European larch (*Larix decidua*) in the Swiss Alps.

During the transition months (April and May), the shift from temperature driven to transpiration-induced diurnal cycle in stem radius is tracked at a daily resolution for both black spruce and larch in Figures 5a, 5d, 6a, and 6d for 2019 and 2020, respectively. Stem radius change for both species follows diurnal changes in air temperature (typical of winter) prior to April 13, 2019 and April 17, 2020. During this period in early spring, large variations in air temperature between day and night also result in large stem radius change amplitudes (Turcotte et al., 2009). This daily stem radius cycle is reversed on April 13 in 2019 and on April 17 in 2020, when stem radius maximum values are observed at predawn and stems have thawed according

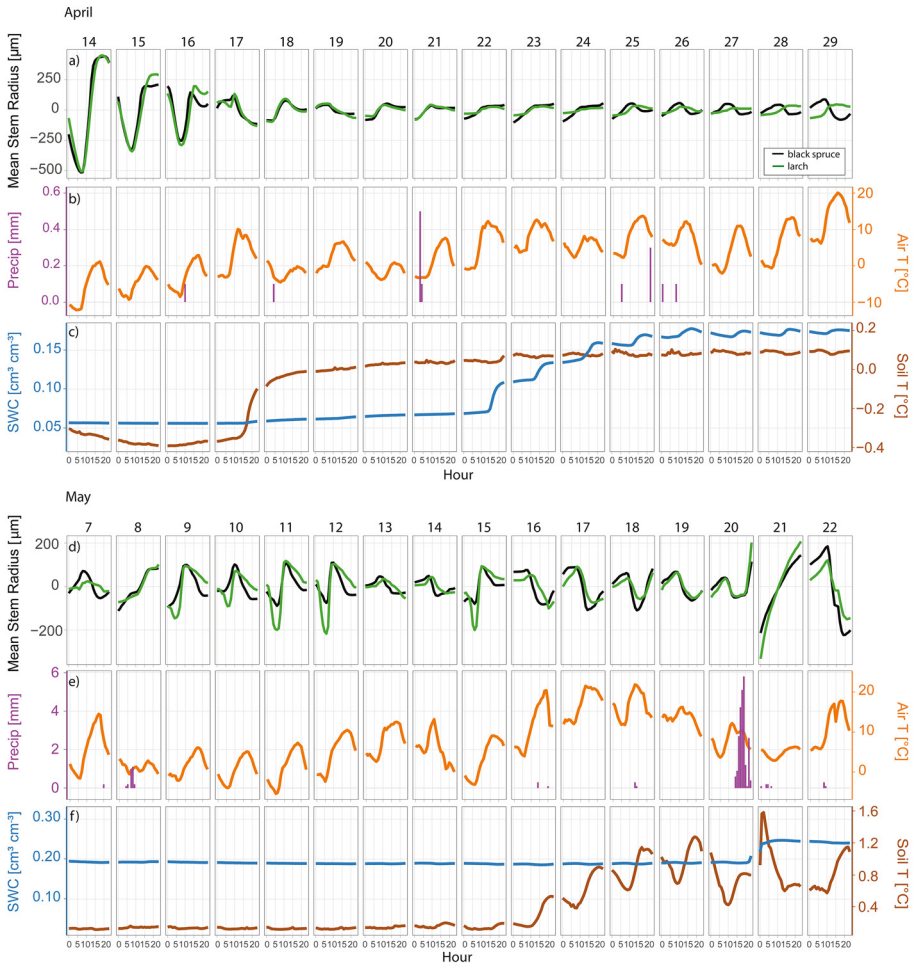

Figure 6. Half-hourly mean environmental variables and stem diurnal cycle during the onset of transpiration in April ((a)–(c)) and May ((d)–(f)) 2020. Panel (a) and (d) show mean stem radius (Mean SR) for black spruce and larch. Panel (b) and (e) show precipitation (Precip) and air temperature (Air T) during same time interval. Lower panels show soil volumetric water content (SWC) and soil temperature (Soil T). The number on the top of each panel indicates the day of the month. SWC, soil volumetric water content.

to ΔD. This indicates the onset of stem rehydration. Rainfall events induced an increase in stem radius and tree water storage refill for both species on April 15 & 16, May 10 & 15, 2019, and May 21, 2020.

Black spruce show a clear onset of the transpiration-induced diurnal cycle in stem radius on April 17 in 2019 and on April 25 in 2020 (Figures 5a and 6a). Larch do not show any clear cycle (beyond occasional stem rehydration) until later in the season, with the onset dates of May 22 in 2019 and May 18 in 2020 (Figures 5d and 6). The switch to a transpiration-induced diurnal cycle on April 17 in black spruce corresponds with the start of the increasing $SIF_{relative}$ signals (Figure 2e and 2f), while the transpiration-induced diurnal cycle in larch corresponds with the timing of the leaf-out, as observed in all larch metrics.

GPP data, reported for 2020, begins to increase around the same time as the switch to a transpiration-driven diurnal cycle in black spruce, and increasing black spruce $SIF_{relative}$ (Figure 3j). Furthermore, it shows a brief dip, consistent with the small dip in $SIF_{relative}$ from May 2 through May 11. GPP then continues to increase after the larch switch to a transpiration-driven diurnal cycle on May 17, while black spruce $SIF_{relative}$ levels off.

Stem radius measurements show the onset of radial growth occurring on June 13 for larch and June 14 for black spruce in 2019 (Figure 2h) and June 8 for black spruce and June 19 for larch in 2020 (Figure 3h). The onset of growth does not correspond with any changes in remotely sensed metrics.

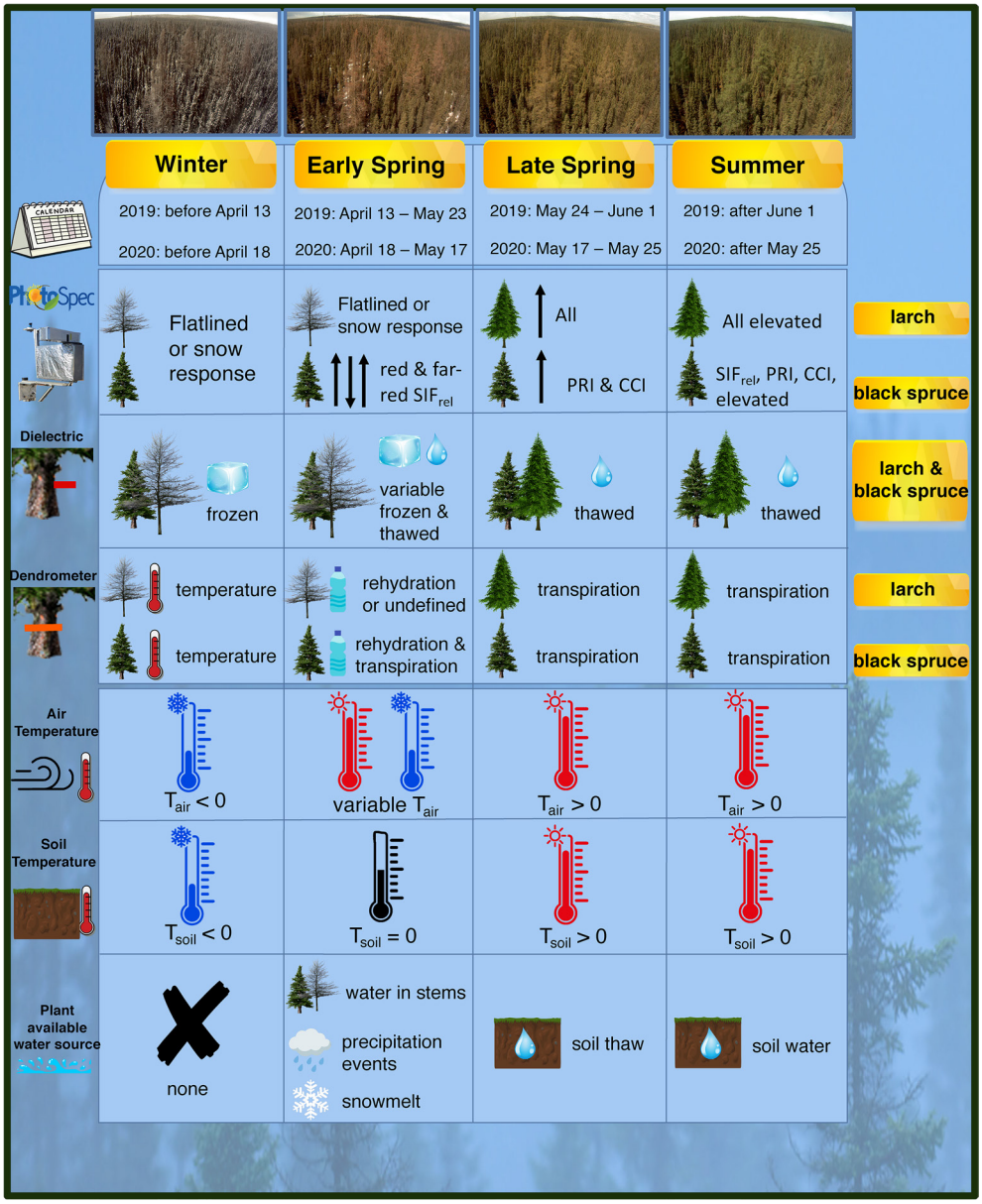

Figure 7. Summary of relevant periods in the winter to summer transition. Shown are relevant dates from 2019 and 2020; measured quantities from PhotoSpec, dielectric probes, and dendrometers; ecophysiologically relevant environmental conditions for each phase.

These results indicate two periods of ecological importance for the spring transition, summarized in the first four rows of Figure 7. We propose the following ecophysiological explanation for this two-phased transition and what each remotely sensed product tells us about the spring transition.

3.2. Evaluation of Remotely Sensed Indices: A Two-Phase Transition

During the spring transition, NDVI and NIRv show no physiologically relevant changes for black spruce which reflects a lack of variation in chlorophyll content throughout the transition (Magney, Bowling, et al., 2019). Both indices do, however, successfully capture the larch leaf-out. NDVI fails to capture photosynthetic activity in evergreen species and has an overall high sensitivity to snow cover (Magney, Bowling, et al., 2019; Stylinski et al., 2002; Gamon et al., 2013) which is reflected in our results. NIRv overcomes the general sensitivity to snow cover (Badgley et al., 2017), making it a useful tool for separating snow and

vegetation signals in the boreal forest where snow cover is particularly prevalent. NIRv scales well at sites where canopy structure co-varies with GPP (Baldocchi et al., 2020; Dechant et al., 2020). This explains why it tracks the larch leaf-out so well but fails to capture photosynthetic reactivation of black spruce, where canopy structure and crown architecture are a minor and de-coupled fraction of carbon uptake (Pappas et al., 2018; Pappas, Maillet, et al., 2020). Because NDVI and NIRv signals are mostly only variable for larch, and more specifically to changes in leaf presence, we suggest that satellite NDVI and NIRv measurements will be largely driven by the growth and senescence of the larch, or other deciduous species in the region. Other measured remotely sensed products (PRI, CCI, and $SIF_{relative}$) show two periods of physiological changes that coincide with changes in stem radius and GPP.

The first phase of the transition is from April 13–May 23, 2019 and April 25–May 17, 2020. It is characterized by a variable $SIF_{relative}$ signal that closely tracks the freeze-thaw state of the stems, slight increases in PRI and CCI, a transpiration-induced cycle in black spruce stem radius measurements, and elevated GPP (summarized in Figure 7). We propose that this first period can be explained by the re-activation of the rapidly reversible xanthophyll cycle and photosynthetic function in black spruce. Changes in black spruce red and far-red $SIF_{relative}$ during this time align closely with the shift from a temperature driven to a water flux driven (both rehydration and transpiration-induced) diurnal cycle in stem radius (Figure 7). Additionally, in 2020, this period coincides with the initial increase in GPP, supporting our use of dendrometers for determining the onset of transpiration and carbon uptake. In spring, the combination of transpiration (as shown by stem radius measurements and supported by GPP) and photosystem II activity (as suggested by increasing $SIF_{relative}$) suggests a change in photochemical efficiency and a reactivation of the rapidly reversible xanthophyll cycle. We, therefore, interpret changes in $SIF_{relative}$ (a proxy for SIF_{yield}) as signifying an increase in photochemistry and a subsequent drop in non-photochemical quenching, consistent with Porcar-Castell et al. (2014). Finally, red and far-red $SIF_{relative}$ signals agree well because at seasonal timescales, the ratio of red to far-red SIF in evergreen needles is primarily determined by chlorophyll concentration (Magney, Frankenberg, et al., 2019), of which we observe little change in black spruce (represented by invariant NDVI and NIRv signals). Therefore, either red or far-red $SIF_{relative}$ will be effective at capturing the first phase of the transition.

Magney, Bowling, et al. (2019) reported an increase in SIF prior to an increase in GPP in a subapline evergreen forest. This is not observed in our results (Figure 3). We suggest that the discontinuity observed by Magney, Bowling, et al. (2019) may be attributable to the fact that GPP is spatially averaged over the flux footprint and will be influenced by recovery of understory following soil thaw and snow melt. Therefore, the recovery of understory may play a less important role at the SOBS site, however, the understory recovery has yet to be explored.

The second phase of the transition is from May 24–June 1, 2019 and May 17–May 25, 2020 (Figure 7). It is characterized by additional increases in PRI and CCI in black spruce, as well as the larch leaf-out and shift to a transpiration-induced stem radius cycle in larch. Based on previous studies connecting PRI and CCI to changes in Chl:Car pigment ratios (Cheng et al., 2020; Filella et al., 2009; Garrity et al., 2011; Porcar-Castell et al., 2012; Stylinski et al., 2002; Wong & Gamon, 2015b), we interpret the increasing black spruce PRI and CCI signals as reflective of a decrease in bulk carotenoid pigments, which indicates a decrease in sustained photoprotection and a more permanent physiological shift for the growing season. Changes in CCI represent the seasonal behavior of Chl:Car pigment ratios (Gamon et al., 2016). Since NDVI is relatively invariant, we assume chlorophyll concentration and canopy structure remain largely stable. Therefore, increases in CCI are driven by a decrease in carotenoid concentrations (Gamon et al., 2016). PRI on the other hand is influenced by three distinct processes: the short term response related to the operation of the xanthophyll cycle, seasonally changing Chl:Car pigment ratios, and a shifting leaf albedo during periods of deep cold (Gamon & Berry, 2012; Wong & Gamon, 2015b). In spring, while the forest experiences both changes in the rapidly reversible xanthophyll cycle and increasing Chl:Car pigment ratios, increasing Chl:Car pigment ratios are the dominant driver of changes in PRI (Filella et al., 2009; Garrity et al., 2011; Porcar-Castell et al., 2012; Stylinski et al., 2002; Wong & Gamon, 2015b). This is why changes in PRI during the first phase of the transition with the reactivation of the xanthophyll cycle are smaller and more variable than the subsequent changes during the second phase.

To further test our interpretation of PRI and a reactivation of the rapidly reversible xanthophyll cycle during the first phase of the spring transition prior to changes in pigment ratios, we analyzed light response curves using the 30 min average data for PRI versus PAR over a 10-day period during winter, spring, and summer in 2019 and 2020 (data not shown). The winter light response curves showed no appreciable change in PRI at high light levels indicative of sustained NPQ, as expected in winter (Gamon & Berry, 2012). Summer PRI light response curves showed a clear decrease in PRI at high light levels, indicative of rapidly reversible NPQ, as expected in summer (Gamon & Berry, 2012). Spring light response curves during all phases of the spring transition were highly variable and therefore inconclusive. We attribute the variability of the spring light response curves to a mixture of offsetting responses to temperature, direct/diffuse light conditions, and viewing direction effects. Given these potential sources of error, and findings from previous studies on drivers of PRI during spring (Porcar-Castell et al., 2012; Wong & Gamon, 2015b), we attribute the changes in PRI as consistent with a shift in bulk Chl:Car pigment ratios, which is further supported by our analysis of CCI.

This two-phased interpretation of the spring transition supports previous work which proposes a decoupling of the reactivation of the diurnal xanthophyll cycle and increasing Chl:Car pigment ratios for evergreens in spring, with the reactivation of the xanthophyll cycle occurring as an early step (Porcar-Castell et al., 2012; Wong & Gamon, 2015a). We observe a slow increase in CCI and PRI during the first phase of the transition. However, these indices don't dramatically increase and level off before the second stage of the spring transition as we observe in the $SIF_{relative}$ signals (Figures 2 and 3). Therefore, we propose that the secondary (and more pronounced) increase in CCI and PRI signifies major changes in the Chl:Car pigment ratios. This change in pigment ratios marks the second stage of the spring transition as a more permanent shift away from sustained photoprotection for the growing season. Finally, we propose that CCI is a more useful measure of seasonal pigments behavior over winter and during the transition seasons compared with PRI due to its resiliency against snow contamination, and its fewer potential drivers.

The onset of radial growth occurs after the two phases of the spring transition and is not captured by any remote sensing metrics in this study. This is consistent with Eitel et al. (2020), who showed changes in PRI prior to radial stem growth and Zweifel et al. (2010), who showed photosynthetic carbon uptake before radial growth in evergreen species. This highlights the inherent inability of remote sensing to account for long-term above ground carbon storage and carbon partitioning following C assimilation through photosynthesis.

3.3. Environmental Drivers of the Spring Transition

3.3.1. Statistical Identification of Important Environmental Drivers

To explore the environmental drivers of the two phases of the spring transition, we used random forest models and a qualitative analysis of environmental conditions and the forest's ecophysiological response. A random forest model was chosen because it is non-parametric and is more suitable for approximating nonlinear relationships in complex systems. We used MATLAB's TreeBagger function to train 1,000 random forest models, each with 100 regression trees using the daily average data from March 20th–June 27th, for 2019 and 2020 separately, to capture the full spring transition and to allow a qualitative comparison with the time series of the 2 years. Input variables were daily averaged PAR, soil volumetric water content (VWC), soil temperature, air temperature, and vapor pressure deficit (VPD). Response variables were either daily averaged red $SIF_{relative}$, far-red $SIF_{relative}$, PRI, or CCI, for both black spruce and larch. We removed all data points that had snow contamination (as identified with visual examination of Phenocam images and indicated in Figure 2). We averaged the unbiased predictor importance estimates and out-of-bag R^2 values of the 1,000 trials to arrive at the data presented in Figure 8.

The random forest model identified important environmental drivers for the spring transition, as characterized by remotely sensed products, shown in Figures 8 and 9. In black spruce, the important predictor variables were different depending on the physiologically sensitive remotely sensed response variable in question, with some small differences between 2019 and 2020. Black spruce red $SIF_{relative}$ in 2019 and black spruce far-red $SIF_{relative}$ in 2019 and 2020 are best predicted by soil temperature, soil VWC, and air temperature (Figures 8a, 8c, and 9c). Black spruce red $SIF_{relative}$ in 2020 has a more even distribution of dependencies,

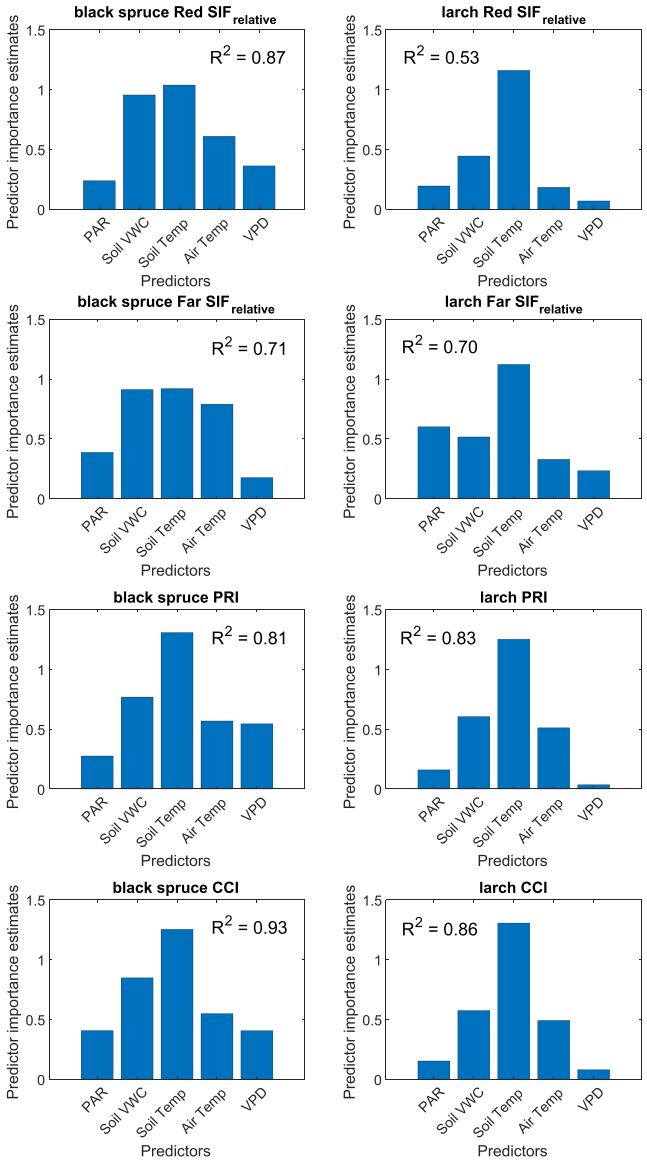

Figure 8. Averaged unbiased predictor importance estimates from 1,000 repetitions of a random forest model from March 20th through June 27th, 2019 for both black spruce and larch with snow days removed.

with soil VWC and soil temperature most important (Figure 9a). We hypothesize that black spruce red $SIF_{relative}$ in 2020 shows slightly different predictor variables than all other $SIF_{relative}$ measurements because it is more poorly predicted ($R^2 = 0.66$) than other $SIF_{relative}$ measurements (black spruce red $SIF_{relative}$ 2019 $R^2 = 0.87$, black spruce far-red $SIF_{relative}$ in 2019 $R^2 = 0.71$, black spruce far-red $SIF_{relative}$ $R^2 = 0.87$). Predictor importances for black spruce PRI and CCI are remarkably similar in 2019 and 2020 and have soil temperature as the most important predictor (Figures 8e, 8g, 9e, and 9g). In 2020, they also show a strong dependency on soil VWC and larger dependencies on air temperature than in 2019. The 2020 dependency is explained by a qualitative analysis of the environmental conditions present in the time series. The random forest model identified soil temperature as the dominant predictor for all larch variables in 2019 and 2020 (Figures 8b, 8d, 8f, 8h, 9b, 9d, 9f and 9h). Additionally, larch variables in 2020 show a greater dependence on soil VWC (Figures 9b, 9d, 9f, and 9h). The results from the random forest analysis support a qualitative analysis of the 2019 and 2020 time series (Figures 2 and 3) and daily breakdowns (Figures 5 and 6), and imply that the two phases of the spring transition are controlled by different environmental conditions as explained below and summarized in Figure 7.

3.3.2. Environmental Drivers of the Two-Phased Transition

3.3.2.1. Phase 1: The Onset of Black Spruce Photosynthesis

The first phase of the spring transition, the onset of black spruce photosynthesis, is marked by changes in black spruce red and far-red $SIF_{relative}$ which were best predicted by soil temperature, soil water content, and air temperature in the random forest model. Figures 2 and 3 show that this period of time for both 2019 and 2020 is characterized by the following environmental conditions: variable air temperatures above and below zero, soil temperatures at zero, and slow increases in soil water content following precipitation events (summarized in Figure 7). During this time, changes in energy balance, including air temperature effects, drive the freeze-thaw state of the stems (Figures 2g, 2i, 3g, and 3i). Soil temperatures are approximately 0°C and do not follow diurnal variations in air temperature as observed later in the season due to the insulating properties of snow and the latent heat of frozen water (Figures 5b and 6b). Soil water content increases during precipitation events on April 14, 15, 16 in 2019, which add water to the soil and aid in snow melt (Figure 5b). Following these precipitation events, we observe rapid stem rehydration shown in Figure 5a, similar to what has been previously observed with stem radius measurements following precipitation events (Kozlowski et al., 1962; Kozlowski & Winget, 1964; Tardif et al., 2001). Finally, increases and decreases in $SIF_{relative}$ closely follow increases and decreases in air temperature and small increases in soil water content during this time (Figures 2e, 2f, 2i, 3e, 3f, and 3i). Therefore, we propose that the first phase of the spring onset is driven by the combination of increases in air temperature above 0°C, which thaws tree stems, coupled with small increases in soil water content, due to either precipitation events or snow melt (Figure 7). These favorable growing conditions drive the onset of photosynthesis in black spruce, and allow it to take advantage of early spring prior to larch leaf-out and the completion of soil thaw.

These results are consistent with previous studies that suggest that frozen stems both constrain the spring recovery and limit photosynthetic activity in winter, therefore making air temperature a key driver of photosynthetic reactivation in boreal systems (Bowling et al., 2018; Ensminger et al., 2004; Sevanto et al., 2006; Tanja et al., 2003). In a boreal Scots pine stand in Finland, the onset of stand photosynthesis was triggered by a rise in air temperature prior to complete soil thaw, much like what is observed at SOBS (Ensminger

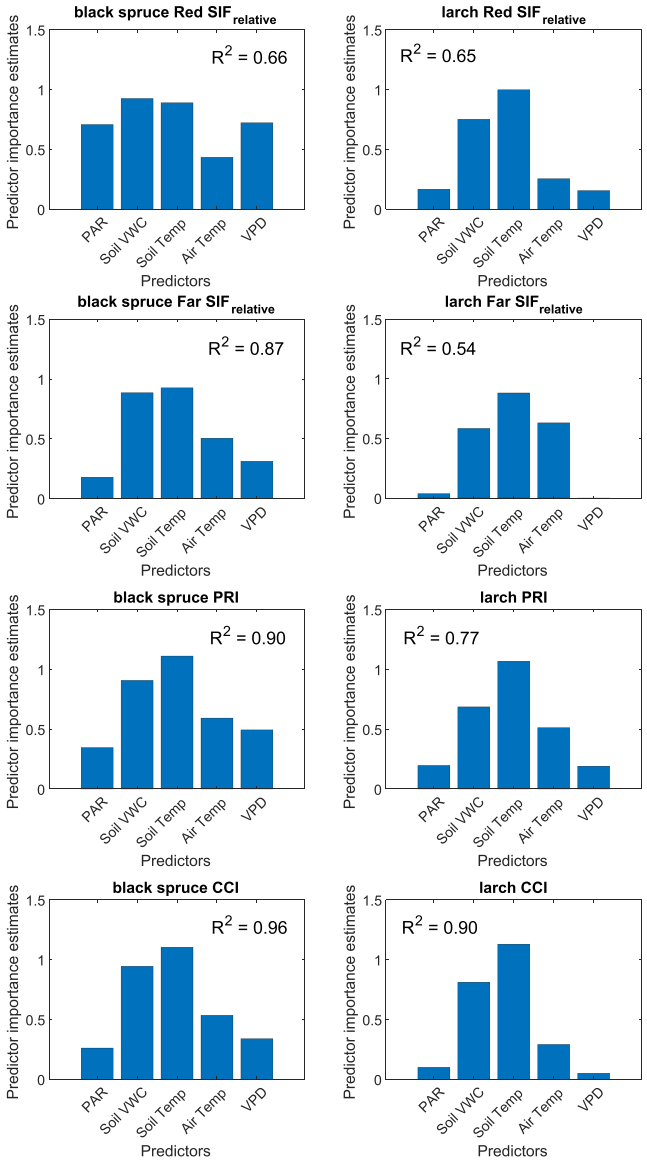

Figure 9. Averaged unbiased predictor importance estimates from 1,000 repetitions of a random forest model from March 20th through June 27th, 2020 for both black spruce and larch with snow days removed.

et al., 2004; Sevanto et al., 2006). Furthermore, the role of frozen stems as a key blockage to the water transport system, beyond availability of water, was highlighted in a Colorado evergreen system by Bowling et al. (2018). At SOBS, spring temperatures have additionally been most closely associated with inter-annual variability in GPP (Liu et al., 2019). This highlights not only the importance of the timing of the spring onset of photosynthesis for the overall carbon balance, but also the importance of air temperature and the timing of stem thaw as important predictors of the spring onset of photosynthesis (Bowling et al., 2018; Liu et al., 2019).

Severe intermittent low-temperature episodes during early spring have been found to not only halt but reverse the physiological recovery (Ensminger et al., 2004). In 2019, a cold snap from April 25–May 1 froze tree stems and led to a subsequent drop in $SIF_{relative}$ (Figures 2e–2g and 2i). This indicates a potential reversal of physiological recovery. There was a similar period of cold in 2020 from May 2–May 11, however, temperatures during this period did not drop well below 0°C, and therefore did not lead to a freeze in the tree stems. The subsequent drop in $SIF_{relative}$ was therefore greatly reduced (Figures 3e–3g and 3i). Increased air temperatures and the freeze/thaw state of the stems alone, however, is insufficient for fully determining the reactivation of photosynthesis. This is highlighted by the difference in timing between stem rehydration and the onset of transpiration in 2019 versus 2020.

In 2019 and 2020, trunk thaw coincided with the timing of stem rehydration in both black spruce and larch (Figures 2 and 3). This further supports the idea that air temperature is a key driver for a tree's access to water, through its influence on stem and soil thawing. In 2019, strong rehydration patterns for both black spruce and larch followed major rainfall events (4.73 mm total) and led to a rapid exponential increase in stem size (Figures 2h and 5a). In 2020, only minor precipitation events (1.79 mm total) occurred and did not lead to the same rapid increase in stem size (Figures 3h and 6a). Therefore, the black spruce transpiration-induced cycle (and increases in $SIF_{relative}$) started only four days after the onset of stem rehydration in 2019 (Figure 2). In 2020, it began 7 days after the onset of stem rehydration and followed a slight increase in available soil VWC. The increase in available soil VWC was likely due to snow melt or soil temperatures reaching a freeze/thaw equilibrium (Figure 3). These observations highlight the importance of accessible soil water content, in addition to thawed stems, for photosynthetic recovery and the role of early spring precipitation events.

Trees are able to access small soil water reservoirs despite partially frozen soils because soil temperatures at (or just below) 0°C do not inhibit photosynthesis or water uptake from the soil (Bergh & Linder, 1999; Sevanto et al., 2006). Frozen soils do, however, limit maximum sap flow and maximum photosynthetic capacity (Bergh & Linder, 1999), which limits the amount of water they are able to extract. This may explain why the spring recovery happens in two distinct steps: before and after complete soil thaw, and why evergreens recover prior to larch leaf-out. Soil temperature was identified as a dominant predictor for $SIF_{relative}$ because by the time soil thaw occurs, $SIF_{relative}$ is already elevated from the first phase of the spring onset, and therefore, soil thaw becomes a good predictor of elevated SIF.

3.3.2.2. Phase 2: Black Spruce Pigment Transitions and Larch Leaf-Out

The second phase of the spring transition is characterized by completely thawed soils (Figure 7). Soil temperature increases above 0°C and begins to follow diurnal changes in air temperature on May 15, 2019 and May 16 2020. Shortly after, we observe changes in black spruce PRI and CCI (Figures 2c, 2d, 3c, and 3d),

as well as larch leaf-out (Figures 2a and 3a) and larch transition to a transpiration-induced diurnal cycle (Figures 5d and 6d). Therefore, complete soil thaw is key for black spruce to make more permanent physiological shifts for the growing season. They do this by increasing Chl:Car pigment ratios and reaching maximum photosynthetic capacity, which is limited under frozen soil conditions (Bergh & Linder, 1999). Furthermore, with water access no longer limited, larch is able to use larger water stores to begin the leaf-out process. In 2020, soil VWC was identified as an important predictor of changes in black spruce PRI, CCI, and larch metrics. Figures 3i and 6f show that shortly after soil thaw occurs in 2020, soil VWC dramatically increases. We therefore attribute increases in soil VWC, after soil thaw, to ice melt, making soil temperature the dominant driver.

Soil thaw as a trigger for the spring photosynthetic onset has previously been reported in deciduous forests (Baldocchi et al., 2005) and in Alaskan boreal systems across varied vegetation types (Parazoo et al., 2018). Early photosynthesis prior to soil thaw, however, was observed in predominantly evergreen systems (Parazoo et al., 2018). We suggest that since GPP-based metrics are spatially integrated, they may show landscape thaw as the dominant predictor for carbon uptake in mixed stand forests due to the influence of deciduous species and understory recovery. Furthermore, this may also impact satellite-based measurements, as the larch and other deciduous species have large crown areas compared with black spruce (Pappas et al., 2018), and therefore may impact the satellite signal much more.

3.4. Further Implications

Our results, and previous work, show the complexities of wintertime photosynthesis and the spring transition in needleleaf forests and uncertainties associated with future warming scenarios. On the one hand, previous work in a boreal forest in Finland has suggested that wintertime rates of photosynthesis in evergreen systems are possible through small water reservoirs stored in the stems (Sevanto et al., 2006). However, Bowling et al. (2018) found no evidence of wintertime photosynthetic activity in an evergreen system in Colorado despite temperatures being warm enough to thaw stems. While we did not explore wintertime photosynthesis, our results suggest that if there are viable sources of water following precipitation events or soil temperatures at 0°C in thermal equilibrium, wintertime photosynthesis may be possible at the SOBS site. We acknowledge that sustained NPQ during winter may maintain the forests dormant state and prohibit photosynthetic activity during winter (Bowling et al., 2018). However, the recovery of SIF and photosynthetic function prior to the shift in bulk pigment ratios suggests a potential, more dynamic, recovery of photosynthetic activity in winter may be possible. On the other hand, a higher variability of freeze-thaw cycles (Mellander et al., 2007) could have serious consequences for tissue mortality during springtime frosts (Richardson et al., 2018), if the combination of thawed trunks and soils leads to an earlier springtime reactivation, as suggested by our results. Frequent pigment sampling or continuous PAM fluorescence (Porcar-Castell et al., 2012) at a daily or sub-daily resolution, both over winter and during the spring recovery, would provide the necessary information on the reactivation of the rapidly reversible xanthophyll cycle during these times. Furthermore, analysis of wintertime dendrometer and dielectric measurements combined with remote sensing metrics may provide a better view of species-specific wintertime photosynthesis than spatially integrated measures.

The variability of the $SIF_{relative}$ signal, and the reversal of photosynthetic recovery due to severe cold weather events (described in Section 3.3.2.1), means that care must be taken during the spring transition to resolve remote sensing signals. Simple break point metrics that determine a "cutoff" date for the spring recovery may fail to capture the dynamic nature of evergreens during this time which may therefore account for many of the uncertainties in the timing and drivers of the spring recovery. Furthermore, in mixed forest stands, the different recovery strategies of deciduous and evergreen species will further complicate a break-point method, and pose significant challenges for spatially integrated measures of the spring recovery such as satellite measurements and EC derived GPP.

Our results highlight the necessity of spatially downscaling remote sensing metrics over diverse landscapes during the spring onset. Based on our results, we propose that satellite signals of NDVI and NIRv will be predominantly driven by deciduous dynamics, although further work is necessary to explore these nuances. Furthermore, prior work (Atherton et al., 2017) has shown how PRI is more variable between species than the biochemical responses of each species individually, which will pose significant complications for PRI

Acknowledgments
This work was supported by NASA's Earth Science Division IDS (awards 80NSSC17K0108 at UCLA, 80NSSC17K0110 at JPL) and ABoVE programs (award 80NSSC19M0130). A portion of this research was carried out at the Jet Propulsion Laboratory, California Institute of Technology, under a contract with the National Aeronautics and Space Administration.
This material is also based upon work supported by the National Science Foundation Graduate Research Fellowship under Grant No. DGE-1650604 and DGE-2034835. Any opinion, findings, and conclusions or recommendations expressed in this material are those of the authors(s) and do not necessarily reflect the views of the National Science Foundation.
DRB and TSM were funded during this time by the Macrosystems Biology and NEON-Enabled Science program at NSF (award 1926090).
We acknowledge funding by the Canadian Space Agency and Natural Sciences and Engineering Research Council of Canada (NSERC). O. Sonnentag was supported through the Canada Research Chairs and Natural Sciences and Engineering Research Council Discovery Grants programs. The meteorological, soil and eddy-covariance measurements at SOBS were made with support from the Global Institute for Water Security, University of Saskatchewan.
The authors thank our many collaborators, including site PIs and technicians, for their efforts in support of PhenoCam. The development of PhenoCam has been funded by the Northeastern States Research Cooperative, NSF's Macrosystems Biology program (awards EF-1065029 and EF-1702697), and DOE's Regional and Global Climate Modeling program (award DE-SC0016011). The authors acknowledge additional support from the US National Park Service Inventory and Monitoring Program and the USA National Phenology Network (grant number G10AP00129 from the United States Geological Survey), and from the USA National Phenology Network and North Central Climate Science Center (cooperative agreement number G16AC00224 from the United States Geological Survey). Additional funding, through the National Science Foundation's LTER program, has supported research at Harvard Forest (DEB-1237491) and Bartlett Experimental Forest (DEB-1114804). The authors also thank the USDA Forest Service Air Resource Management program and the National Park Service Air Resources program for contributing their camera imagery to the PhenoCam archive.

from satellite measurements. The PRI signals of black spruce and larch agree well in our study, however, further work is necessary to understand how spatial averaging of this data complicates our understanding of LUE and pigment transitions. Finally, species specific responses are spatially averaged in GPP and pose a significant challenge for breaking down the SIF/GPP relationship in mixed forest stands. The larger crown area of deciduous species may contribute to a much higher SIF signal than evergreen species, despite contributing less to the GPP signal. Future work combining dendrometer, GPP, and remote sensing metrics will help to clarify the role that individual species play in these signals.

4. Conclusions

We explored the efficacy of remotely sensed metrics for determining the spring transition for deciduous and evergreen species in the boreal forest and examined environmental controls for the spring transition. We found that evergreen black spruce experience a two-phase spring transition which can be observed using remote sensing metrics, and that these two phases have different environmental controls. The first phase of the transition, the onset of photosynthesis, was detected with relative solar-induced chlorophyll fluorescence and depended on warm air temperatures to thaw the tree stems and an increase in plant available water content in the soil through snow-melt or precipitation events. The second phase of the transition, the change in bulk pigment ratios, was detected with vegetation indices PRI and CCI and began after the soil had completely thawed which gave trees greater access to water stored in the soil. Deciduous larch depended on soil thaw for leaf-out and all remotely sensed metrics were able to detect the leaf-out. We suggest that inter-species differences in the timing and drivers of the spring transition contained in integrated GPP-based estimates, or spatially averaged satellite signals, may account for many of the differences and disagreements on the timing and drivers of the spring transition in existing literature. Therefore, incorporating trait information into such estimates is essential for understanding why these differences exist. Finally, our results highlight the value of a multivariate approach combining continuous tree-level observations with tower-based remote sensing products as a way to study physiological processes on a tree-by-tree basis. This approach provides insight into the drivers of spatially averaged EC measurements and satellite observations.

Data Availability Statement

PhotoSpec SIF and VI are available at https://doi.org/10.5281/zenodo.4637567. Environmental and eddy covariance and data are available at https://doi.org/10.20383/101.0300. Dielectric data are available at https://doi.org/10.5683/SP2/GUBS0N. Stem radius data are available at https://doi.org/10.20383/102.0367.

References

Adams, W. W., Demmig-Adams, B., Rosenstiel, T. N., Brightwell, A. K., & Ebbert, V. (2002). Photosynthesis and photoprotection in overwintering plants. *Plant Biology*, *4*(5), 545–557. https://doi.org/10.1055/s-2002-35434

Adams, W. W., Zarter, C. R., Ebbert, V., & Demmig-Adams, B. (2004). Photoprotective Strategies of Overwintering Evergreens. *BioScience*, *54*(1), 41–49. https://doi.org/10.1641/0006-3568(2004)054[0041:psooe]2.0.co;2

Améglio, T., Cochard, H., Ewers, F. W., Pascal, B., & Crouelle, S. I. D. (2001). Stem diameter variations and cold hardiness in walnut trees. *Journal of Experimental Botany*, *52*(364), 2135–2142. https://doi.org/10.1093/jexbot/52.364.2135

Atherton, J., Olascoaga, B., Alonso, L., & Porcar-Castell, A. (2017). Spatial variation of leaf optical properties in a boreal forest is influenced by species and light environment. *Frontiers of Plant Science*, *8*, 309. https://doi.org/10.3389/fpls.2017.00309

Badgley, G., Anderegg, L. D. L., Berry, J. A., & Field, C. B. (2019). Terrestrial gross primary production: Using NIR V to scale from site to globe. *Global Change Biology*, *25*(11), 3731–3740. https://doi.org/10.1111/gcb.14729

Badgley, G., Field, C. B., & Berry, J. A. (2017). Canopy near-infrared reflectance and terrestrial photosynthesis. *Science Advances*, *3*(3), e1602244. https://doi.org/10.1126/sciadv.1602244

Baldocchi, D. D. (2003). Assessing the eddy covariance technique for evaluating carbon dioxide exchange rates of ecosystems: Past, present and future. *Global Change Biology*, *9*(4), 479–492. https://doi.org/10.1046/j.1365-2486.2003.00629.x

Baldocchi, D. D., Black, T. A., Curtis, P. S., Falge, E., Fuentes, J. D., Granier, A., et al. (2005). Predicting the onset of net carbon uptake by deciduous forests with soil temperature and climate data: A synthesis of FLUXNET data. *International Journal of Biometeorology*, *49*(6), 377–387. https://doi.org/10.1007/s00484-005-0256-4

Baldocchi, D. D., Hincks, B. B., & Meyers, T. P. (1988). Measuring biosphere-atmosphere exchanges of biologically related gases with micrometeorological methods. *Ecology*, *69*(5), 1331–1340. https://doi.org/10.2307/1941631

Baldocchi, D. D., Ryu, Y., Dechant, B., Eichelmann, E., Hemes, K., Ma, S., et al. (2020). Outgoing near-infrared radiation from vegetation scales with canopy photosynthesis across a spectrum of function, structure, physiological capacity, and weather. *Journal of Geophysical Research: Biogeosciences*, *125*(7). https://doi.org/10.1029/2019JG005534

Barr, A. G., Black, T. A., Hogg, E. H., Kljun, N., Morgenstern, K., & Nesic, Z. (2004). Inter-annual variability in the leaf area index of a boreal aspen-hazelnut forest in relation to net ecosystem production. *Agricultural and Forest Meteorology*, *126*(3–4), 237–255. https://doi.org/10.1016/j.agrformet.2004.06.011

Barr, A. G., Morgenstern, K., Black, T. A., McCaughey, J. H., & Nesic, Z. (2006). Surface energy balance closure by the eddy-covariance method above three boreal forest stands and implications for the measurement of the CO2 flux. *Agricultural and Forest Meteorology*, *140*(1–4), 322–337. https://doi.org/10.1016/j.agrformet.2006.08.007

Bergh, J., & Linder, S. (1999). Effects of soil warming during spring on photosynthetic recovery in boreal Norway spruce stands. *Global Change Biology*, *5*(3), 245–253. https://doi.org/10.1046/j.1365-2486.1999.00205.x

Bonan, G. B. (2008). Forests and climate change: Forcings, feedbacks, and the climate benefits of forests. *Science*, *320*(5882), 1444–1449. https://doi.org/10.1126/science.1155121

Bowling, D. R., Logan, B. A., Hufkens, K., Aubrecht, D. M., Richardson, A. D., Burns, S. P., et al. (2018). Limitations to winter and spring photosynthesis of a Rocky Mountain subalpine forest. *Agricultural and Forest Meteorology*, *252*, 241–255. https://doi.org/10.1016/j.agrformet.2018.01.025

Chen, J. M., Govind, A., Sonnentag, O., Zhang, Y., Barr, A., & Amiro, B. (2006). Leaf area index measurements at Fluxnet-Canada forest sites. *Agricultural and Forest Meteorology*, *140*(1–4), 257–268. https://doi.org/10.1016/j.agrformet.2006.08.005

Cheng, R., Magney, T. S., Dutta, D., Bowling, D. R., Logan, B. A., Burns, S. P., et al. (2020). Decomposing reflectance spectra to track gross primary production in a subalpine evergreen forest. *Biogeosciences*, *17*(18), 4523–4544. https://doi.org/10.5194/bg-17-4523-2020

Commane, R., Lindaas, J., Benmergui, J., Luus, K. A., Chang, R. Y.-W., Daube, B. C., et al. (2017). Carbon dioxide sources from Alaska driven by increasing early winter respiration from Arctic tundra. *Proceedings of the National Academy of Sciences of the United States of America*, *114*(21), 5361–5366. https://doi.org/10.1073/pnas.1618567114

De Swaef, T., De Schepper, V., Vandegehuchte, M. W., & Steppe, K. (2015). Stem Diameter variations as a versatile research tool in ecophysiology, 35(No. 10). Oxford University Press. https://doi.org/10.1093/treephys/tpv080

Dechant, B., Ryu, Y., Badgley, G., Zeng, Y., Berry, J. A., Zhang, Y., et al. (2020). Canopy structure explains the relationship between photosynthesis and sun-induced chlorophyll fluorescence in crops. *Remote Sensing of Environment*, *241*, 111733. https://doi.org/10.1016/j.rse.2020.111733

Drew, D. M., & Downes, G. M. (2009). The use of precision dendrometers in research on daily stem size and wood property variation: A review. *Dendrochronologia*, *27*(2), 159–172. https://doi.org/10.1016/j.dendro.2009.06.008

Eitel, J. U. H., Griffin, K. L., Boelman, N. T., Maguire, A. J., Meddens, A. J. H., Jensen, J., et al. (2020). Remote sensing tracks daily radial wood growth of evergreen needleleaf trees. *Global Change Biology*, *26*(7), 4068–4078. https://doi.org/10.1111/gcb.15112

Eller, C. B., Barros, F. de V., Bittencourt, P. R. L., Rowland, L., Mencuccini, M., & Oliveira, R. S.(2018). Xylem hydraulic safety and construction costs determine tropical tree growth. *Plant, Cell and Environment*, *41*(3), 548–562. https://doi.org/10.1111/pce.13106

Ensminger, I., Sveshnikov, D., Campbell, D. A., Funk, C., Jansson, S., Lloyd, J., et al. (2004). Intermittent low temperatures constrain spring recovery of photosynthesis in boreal Scots pine forests. *Global Change Biology*, *10*(6), 995–1008. https://doi.org/10.1111/j.1365-2486.2004.00781.x

Filella, I., Peñuelas, J., Llorens, L., & Estiarte, M. (2004). Reflectance assessment of seasonal and annual changes in biomass and CO2 uptake of a Mediterranean shrubland submitted to experimental warming and drought. *Remote Sensing of Environment*, *90*(3), 308–318. https://doi.org/10.1016/j.rse.2004.01.010

Filella, I., Porcar-Castell, A., Munné-Bosch, S., Bäck, J., Garbulsky, M. F., & Peñuelas, J. (2009). PRI assessment of long-term changes in carotenoids/chlorophyll ratio and short-term changes in de-epoxidation state of the xanthophyll cycle. *International Journal of Remote Sensing*, *30*(17), 4443–4455. https://doi.org/10.1080/01431160802575661

Fisher, J. B., Hayes, D. J., Schwalm, C. R., Huntzinger, D. N., Stofferahn, E., Schaefer, K., et al. (2018). Missing pieces to modeling the Arctic-Boreal puzzle. *Environmental Research Letters*, *13*(2), 020202. https://doi.org/10.1088/1748-9326/aa9d9a

Fu, Z., Stoy, P. C., Luo, Y., Chen, J., Sun, J., Montagnani, L., et al. (2017). Climate controls over the net carbon uptake period and amplitude of net ecosystem production in temperate and boreal ecosystems. *Agricultural and Forest Meteorology*, *243*, 9–18. https://doi.org/10.1016/j.agrformet.2017.05.009

Gamon, J. A., & Berry, J. A. (2012). Facultative and constitutive pigment effects on the Photochemical Reflectance Index (PRI) in sun and shade conifer needles. *Israel Journal of Plant Sciences*, *60*(1–2), 85–95. https://doi.org/10.1560/IJPS.60.1-2.85

Gamon, J. A., Huemmrich, K. F., Stone, R. S., & Tweedie, C. E. (2013). Spatial and temporal variation in primary productivity (NDVI) of coastal Alaskan tundra: Decreased vegetation growth following earlier snowmelt. *Remote Sensing of Environment*, *129*, 144–153. https://doi.org/10.1016/j.rse.2012.10.030

Gamon, J. A., Huemmrich, K. F., Wong, C. Y. S., Ensminger, I., Garrity, S., Hollinger, D. Y., et al. (2016). A remotely sensed pigment index reveals photosynthetic phenology in evergreen conifers. *Proceedings of the National Academy of Sciences of the United States of America*, *113*(46), 13087–13092. https://doi.org/10.1073/pnas.1606162113

Gamon, J. A., Peñuelas, J., & Field, C. B. (1992). A narrow-waveband spectral index that tracks diurnal changes in photosynthetic efficiency. *Remote Sensing of Environment*, *41*(1), 35–44. https://doi.org/10.1016/0034-4257(92)90059-S

Gamon, J. A., Serrano, L., & Surfus, J. S. (1997). The photochemical reflectance index: An optical indicator of photosynthetic radiation use efficiency across species, functional types, and nutrient levels. *Oecologia*, *112*(4), 492–501. https://doi.org/10.1007/s004420050337

Garbulsky, M. F., Peñuelas, J., Papale, D., Ardö, J., Goulden, M. L., Kiely, G., et al. (2010). Patterns and controls of the variability of radiation use efficiency and primary productivity across terrestrial ecosystems. *Global Ecology and Biogeography*, *19*(2), 253–267. https://doi.org/10.1111/j.1466-8238.2009.00504.x

Garrity, S. R., Eitel, J. U. H., & Vierling, L. A. (2011). Disentangling the relationships between plant pigments and the photochemical reflectance index reveals a new approach for remote estimation of carotenoid content. *Remote Sensing of Environment*, *115*(2), 628–635. https://doi.org/10.1016/j.rse.2010.10.007

Gaumont-Guay, D., Black, T. A., Barr, A. G., Griffis, T. J., Jassal, R. S., Krishnan, P., et al. (2014). Eight years of forest-floor CO2 exchange in a boreal black spruce forest: Spatial integration and long-term temporal trends. *Agricultural and Forest Meteorology*, *184*, 25–35. https://doi.org/10.1016/j.agrformet.2013.08.010

Gilmore, A. M., & Ball, M. C. (2000). Protection and storage of chlorophyll in overwintering evergreens. Technical report No. 20, *97*. https://doi.org/10.1073/pnas.150237697

Gitelson, A. A., & Gamon, J. A. (2015). The need for a common basis for defining light-use efficiency: Implications for productivity estimation. *Remote Sensing of Environment*, *156*, 196–201. https://doi.org/10.1016/j.rse.2014.09.017

Goetz, S. J., Bunn, A. G., Fiske, G. J., & Houghton, R. A. (2005). Satellite-observed photosynthetic trends across boreal North America associated with climate and fire disturbance. Technical report. No. 38, *102*. https://doi.org/10.1073/pnas.0506179102

Grossmann, K., Frankenberg, C., Magney, T. S., Hurlock, S. C., Seibt, U., & Stutz, J. (2018). PhotoSpec: A new instrument to measure spatially distributed red and far-red solar-induced chlorophyll fluorescence. *Remote Sensing of Environment*, *216*(November 2017), 311–327. https://doi.org/10.1016/j.rse.2018.07.002

He, L., Magney, T., Dutta, D., Yin, Y., Köhler, P., Grossmann, K., et al. (2020). From the ground to space: Using solar-induced chlorophyll fluorescence to estimate crop productivity. *Geophysical Research Letters*, *47*(7), e2020GL087474. https://doi.org/10.1029/2020GL087474

Jeong, S.-J., Ho, C.-H., Gim, H.-J., & Brown, M. E. (2011). Phenology shifts at start vs. end of growing season in temperate vegetation over the Northern Hemisphere for the period 1982–2008. *Global Change Biology*, *17*(7), 2385–2399. https://doi.org/10.1111/j.1365-2486.2011.02397.x

Jeong, S.-J., Schimel, D., Frankenberg, C., Drewry, D. T., Fisher, J. B., Verma, M., et al. (2017). Application of satellite solar-induced chlorophyll fluorescence to understanding large-scale variations in vegetation phenology and function over northern high latitude forests. *Remote Sensing of Environment*, *190*, 178–187. https://doi.org/10.1016/j.rse.2016.11.021

King, G., Fonti, P., Nievergelt, D., Büntgen, U., & Frank, D. (2013). Climatic drivers of hourly to yearly tree radius variations along a 6°C natural warming gradient. *Agricultural and Forest Meteorology*, *168*, 36–46. https://doi.org/10.1016/j.agrformet.2012.08.002

Kozlowski, T. T., & Winget, C. H. (1964). Diurnal and seasonal variation in radii of tree stems. *Ecology*, *45*(1), 149–155. https://doi.org/10.2307/1937115

Kozlowski, T. T., Winget, C. H., & Torrie, J. H. (1962). Daily Radial Growth of Oak in Relation to Maximum and Minimum Temperature (124(1), pp. 9–17). The University of Chicago Press.

Liu, P., Black, T. A., Jassal, R. S., Zha, T., Nesic, Z., Barr, A. G., et al. (2019). Divergent long-term trends and interannual variation in ecosystem resource use efficiencies of a southern boreal old black spruce forest 1999–2017. *Global Change Biology*, *25*(9), 3056–3069. https://doi.org/10.1111/gcb.14674

Loris, K., Havranek, W. M., & Wieser, G. (1999). The ecological significance of thickness changes in stem, branches and twigs of Pinus cembra L. during winter. *Phyton-Horn*, *39*(4), 117–122.

Luus, K. A., Commane, R., Parazoo, N. C., Benmergui, J., Euskirchen, E. S., Frankenberg, C., et al. (2017). Tundra photosynthesis captured by satellite-observed solar-induced chlorophyll fluorescence. *Geophysical Research Letters*, *44*(3), 1564–1573. https://doi.org/10.1002/2016GL070842

Magney, T. S., Bowling, D. R., Logan, B. A., Grossmann, K., Stutz, J., Blanken, P. D., et al. (2019). Mechanistic evidence for tracking the seasonality of photosynthesis with solar-induced fluorescence. *Proceedings of the National Academy of Sciences of the United States of America*, *116*(24), 11640–11645. https://doi.org/10.1073/pnas.1900278116

Magney, T. S., Frankenberg, C., Köhler, P., North, G., Davis, T. S., Dold, C., et al. (2019). Disentangling changes in the spectral shape of chlorophyll fluorescence: Implications for remote sensing of photosynthesis. *Journal of Geophysical Research: Biogeosciences*, *124*(6), 1491–1507. https://doi.org/10.1029/2019JG005029

Matheny, A. M., Bohrer, G., Garrity, S. R., Morin, T. H., Howard, C. J., & Vogel, C. S. (2015). Observations of stem water storage in trees of opposing Hydraulic strategies. *Ecosphere*, *6*(9), art165. https://doi.org/10.1890/ES15-00170.1

Mellander, P.-E., Löfvenius, M. O., & Laudon, H. (2007). Climate change impact on snow and soil temperature in boreal Scots pine stands. *Climatic Change*, *85*(1–2), 179–193. https://doi.org/10.1007/s10584-007-9254-3

Oh, S., Adams, W. W., Demmig-Adams, B., & Koh, S. C. (2013). Seasonal photoprotective responses in needles of Korean fir (abies Koreana) over an altitudinal gradient on Mount Halla, Jeju Island, Korea. *Arctic Antarctic and Alpine Research*, *45*, 238. https://doi.org/10.1657/1938-4246-45.2.238

Öquist, G., & Huner, N. P. A. (2003). Photosynthesis of over wintering ever green plants. *Annual Review of Plant Biology*, *54*, 329–355. https://doi.org/10.1146/annurev.arplant.54.072402.115741

Ottander, C., Campbell, D., & Öquist, G. (1995). Seasonal changes in photosystem II organisation and pigment composition in Pinus sylvestris. *Planta*, *197*. https://doi.org/10.1007/BF00239954

Pappas, C., Maillet, J., Rakowski, S., Baltzer, J. L., Barr, A. G., Black, T. A., et al. (2020). Aboveground tree growth is a minor and decoupled fraction of boreal forest carbon input. *Agricultural and Forest Meteorology*, *290*, 108030. https://doi.org/10.1016/j.agrformet.2020.108030

Pappas, C., Matheny, A. M., Baltzer, J. L., Barr, A. G., Black, T. A., Bohrer, G., et al. (2018). Boreal tree hydrodynamics: Asynchronous, diverging, yet complementary. *Tree Physiology*, *38*(7), 953–964. https://doi.org/10.1093/treephys/tpy043

Pappas, C., Peters, R. L., & Fonti, P. (2020). Linking variability of tree water use and growth with species resilience to environmental changes. *Ecography*, *43*(9), 1386–1399. https://doi.org/10.1111/ecog.04968

Parazoo, N. C., Arneth, A., Pugh, T. A. M., Smith, B., Steiner, N., Luus, K., et al. (2018). Spring photosynthetic onset and net CO2 uptake in Alaska triggered by landscape thawing. *Global Change Biology*, *24*(8), 3416–3435. https://doi.org/10.1111/gcb.14283

Parazoo, N. C., Magney, T., Norton, A., Raczka, B., Bacour, C., Maignan, F., et al. (2020). Wide discrepancies in the magnitude and direction of modeled solar-induced chlorophyll fluorescence in response to light conditions. *Biogeosciences*, *17*(13), 3733–3755. https://doi.org/10.5194/bg-17-3733-2020

Pearce, R. (2001). Plant freezing and damage. *Annals of Botany*, *87*, 417–424. https://doi.org/10.1006/anbo.2000.1352

Peng, S., Ciais, P., Chevallier, F., Peylin, P., Cadule, P., Sitch, S., et al. (2014). Global Biogeochemical Cycles simulated by terrestrial ecosystem models. *Global Biogeochemical Cycles*, *29*, 46–64. https://doi.org/10.1002/2014GB004931.Received

Perämäki, M., Nikinmaa, E., Sevanto, S., Ilvesniemi, H., Siivola, E., Hari, P., & Vesala, T. (2001). *Tree stem diameter variations and transpiration in Scots pine: An analysis using a dynamic sap flow model*. (pp. 889–897). Holbrook 1995.

Porcar-Castell, A., Garcia-Plazaola, J. I., Nichol, C. J., Kolari, P., Olascoaga, B., Kuusinen, N., et al. (2012). Physiology of the seasonal relationship between the photochemical reflectance index and photosynthetic light use efficiency. *Oecologia*, *170*(2), 313–323. https://doi.org/10.1007/s00442-012-2317-9

Porcar-Castell, A., Tyystjärvi, E., Atherton, J., Van Der Tol, C., Flexas, J., Pfündel, E. E., et al. (2014). Linking chlorophyll, a fluorescence to photosynthesis for remote sensing applications: Mechanisms and challenges. *Journal of Experimental Botany*, *65*(15), 4065–4095. https://doi.org/10.1093/jxb/eru191

Reich, P. B. (2014). The world-wide "fast-slow" plant economics spectrum: A traits manifesto. *Journal of Ecology*, *102*(2), 275–301. https://doi.org/10.1111/1365-2745.12211

Richardson, A. D., Anderson, R. S., Arain, M. A., Barr, A. G., Bohrer, G., Chen, G., et al. (2012). Terrestrial biosphere models need better representation of vegetation phenology: Results from the North American carbon program site synthesis. *Global Change Biology*, *18*(2), 566–584. https://doi.org/10.1111/j.1365-2486.2011.02562.x

Richardson, A. D., Andy Black, T., Ciais, P., Delbart, N., Friedl, M. A., Gobron, N., et al. (2010). Influence of spring and autumn phenological transitions on forest ecosystem productivity. *Philosophical Transactions of the Royal Society B*, *365*(1555), 3227–3246. https://doi.org/10.1098/rstb.2010.0102

Richardson, A. D., Hufkens, K., Milliman, T., Aubrecht, D. M., Furze, M. E., Seyednasrollah, B., et al. (2018). Ecosystem warming extends vegetation activity but heightens vulnerability to cold temperatures. *Nature*, *560*(7718), 368–371. https://doi.org/10.1038/s41586-018-0399-1

Roy, A., Toose, P., Mavrovic, A., Pappas, C., Royer, A., Derksen, C., et al. (2020). L-Band response to freeze/thaw in a boreal forest stand from ground- and tower-based radiometer observations. *Remote Sensing of Environment*, *237*, 111542. https://doi.org/10.1016/j.rse.2019.111542

Schaefer, K., Lantuit, H., Romanovsky, V. E., Schuur, E. A. G., & Witt, R. (2014). The impact of the permafrost carbon feedback on global climate. *Environmental Research Letters*, *9*(8), 085003. https://doi.org/10.1088/1748-9326/9/8/085003

Sevanto, S., Suni, T., Pumpanen, J., Grönholm, T., Kolari, P., Nikinmaa, E., et al. (2006). Wintertime photosynthesis and water uptake in a boreal forest. *Tree Physiology*, (*26*(6), pp. 749–757). Publisher: Oxford Academic. https://doi.org/10.1093/treephys/26.6.749

Sims, D., Luo, H., Hastings, S., Oechel, W., Rahman, A., & Gamon, J. (2006). Parallel adjustments in vegetation greenness and ecosystem CO2 exchange in response to drought in a Southern California chaparral ecosystem. *Remote Sensing of Environment*, *103*(3), 289–303. https://doi.org/10.1016/j.rse.2005.01.020

Sims, D. A., Rahman, A. F., Cordova, V. D., El-Masri, B. Z., Baldocchi, D. D., Flanagan, L. B., et al. (2006). On the use of MODIS EVI to assess gross primary productivity of North American ecosystems. *Journal of Geophysical Research*, *111*(4). https://doi.org/10.1029/2006JG000162

Springer, K., Wang, R., & Gamon, J. (2017). Parallel seasonal patterns of photosynthesis, fluorescence, and reflectance indices in boreal trees. *Remote Sensing*, *9*(7), 691. https://doi.org/10.3390/rs9070691

Steppe, K., De Pauw, D. J. W., Lemeur, R., & Vanrolleghem, P. a. (2006). A mathematical model linking tree sap flow dynamics to daily stem diameter fluctuations and radial stem growth. *Tree Physiology*, *26*(3), 257–273. https://doi.org/10.1093/treephys/26.3.257

Stylinski, C., Gamon, J., & Oechel, W. (2002). Seasonal patterns of reflectance indices, carotenoid pigments and photosynthesis of evergreen chaparral species. *Oecologia*, *131*(3), 366–374. https://doi.org/10.1007/s00442-002-0905-9

Tanja, S., Berninger, F., Vesala, T., Markkanen, T., Hari, P., Mäkelä, A., et al. (2003). Air temperature triggers the recovery of evergreen boreal forest photosynthesis in spring. *Global Change Biology*, *9*(10), 1410–1426. https://doi.org/10.1046/j.1365-2486.2003.00597.x

Tardif, J., Flannigan, M., & Bergeron, Y. (2001). An analysis of the daily radial activity of 7 boreal tree species, northwestern quebec. *Environmental Monitoring and Assessment*, *67*, 141–160. https://doi.org/10.1023/a:1006430422061

Thurner, M., Beer, C., Santoro, M., Carvalhais, N., Wutzler, T., Schepaschenko, D., et al. (2014). Carbon stock and density of northern boreal and temperate forests. *Global Ecology and Biogeography*, *23*(3), 297–310. https://doi.org/10.1111/geb.12125

Tucker, C. J. (1979). Red and photographic infrared linear combinations for monitoring vegetation. *Remote Sensing of Environment*, *8*(2), 127–150. https://doi.org/10.1016/0034-4257(79)90013-0

Turcotte, A., Morin, H., Krause, C., Deslauriers, A., & Thibeault-Martel, M. (2009). The timing of spring rehydration and its relation with the onset of wood formation in black spruce. *Agricultural and Forest Meteorology*, *149*(9), 1403–1409. https://doi.org/10.1016/j.agrformet.2009.03.010

Verhoeven, A. (2014). Sustained energy dissipation in winter evergreens, 201(No. 1). https://doi.org/10.1111/nph.12466

Walther, S., Voigt, M., Thum, T., Gonsamo, A., Zhang, Y., Köhler, P., et al. (2016). Satellite chlorophyll fluorescence measurements reveal large-scale decoupling of photosynthesis and greenness dynamics in boreal evergreen forests. *Global Change Biology*, *22*(9), 2979–2996. https://doi.org/10.1111/gcb.13200

Wang, B., Tian, Z., Zhang, W., Chen, G., Guo, Y., & Wang, M. (2019). Retrieval of green-up onset date from MODIS Derived NDVI in grasslands of inner Mongolia. *IEEE Access*, *7*, 77885–77893. https://doi.org/10.1109/ACCESS.2019.2922003

Wisniewski, M., Gusta, L., & Neuner, G. (2014). Adaptive mechanisms of freeze avoidance in plants: A brief update. *Environmental and Experimental Botany*, *99*, 133–140. https://doi.org/10.1016/j.envexpbot.2013.11.011

Wong, C. Y. S., & Gamon, J. A. (2015a). The photochemical reflectance index provides an optical indicator of spring photosynthetic activation in evergreen conifers. *New Phytologist*, *206*(1), 196–208. https://doi.org/10.1111/nph.13251

Wong, C. Y. S., & Gamon, J. A. (2015b). Three causes of variation in the photochemical reflectance index (PRI) in evergreen conifers. *New Phytologist*, *206*(1), 187–195. https://doi.org/10.1111/nph.13159

Wu, J., Guan, D., Yuan, F., Wang, A., & Jin, C. (2013). Soil temperature triggers the onset of photosynthesis in korean pine. *PloS One*, *8*(6), e65401. https://doi.org/10.1371/journal.pone.0065401

Yang, H., Yang, X., Heskel, M., Sun, S., & Tang, J. (2017). Seasonal variations of leaf and canopy properties tracked by ground-based NDVI imagery in a temperate forest. *Scientific Reports*, *7*(1). https://doi.org/10.1038/s41598-017-01260-y

Zweifel, R. (2016). *Radial stem variations – a source of tree physiological information not fully exploited yet* (pp. 231–232). https://doi.org/10.1111/pce.12613

Zweifel, R., Eugster, W., Etzold, S., Dobbertin, M., Buchmann, N., & Häsler, R. (2010). Link between continuous stem radius changes and net ecosystem productivity of a subalpine Norway spruce forest in the Swiss Alps. *New Phytologist*, *187*(3), 819–830. https://doi.org/10.1111/j.1469-8137.2010.03301.x

Zweifel, R., Haeni, M., Buchmann, N., & Eugster, W. (2016). Are trees able to grow in periods of stem shrinkage? *New Phytologist*, *211*(3), 839–849. https://doi.org/10.1111/nph.13995

Zweifel, R., & Häsler, R. (2000). Frost-induced reversible shrinkage of bark of mature subalpine conifers. *Agricultural and Forest Meteorology*, *102*, 213–222. https://doi.org/10.1016/s0168-1923(00)00135-0

Zweifel, R., & Häsler, R. (2001). *Dynamics of water storage in mature subalpine picea abies: Temporal and spatial patterns of change in stem radius* (pp. 561–569).